MAX-PLANCK-INSTITUT FÜR PLASMAPHYSIK

GARCHING BEI MÜNCHEN

Observation with the Low Energy Neutral Analyser (LENA) on ASDEX

Part I: Ohmic Discharges

Henning Verbeek and the ASDEX-Team

IPP 9/84 February 1991

Die nachstehende Arbeit wurde im Rahmen des Vertrages zwischen dem Max-Planck-Institut für Plasmaphysik und der Europäischen Atomgemeinschaft über die Zusammenarbeit auf dem Gebiete der Plasmaphysik durchgeführt.

Henning Verbeek

February 1991

IPP 9/84

Observations with the Low Energy Neutral Analyzer (LENA) on ASDEX

Part I: Ohmic Discharges

Abstract

This report is a compilation of the observations with the Low Energy Neutral Particle Analyzers (LENA) at ASDEX during Ohmic discharges. The dependence of the energy distributions, the integrated fluxes, and their mean energies on various plasma parameters is documented. Connections and correlations with other edge and divertor diagnostics are discussed.

Contents

1. Introduction

In the last experimental periods of ASDEX we operated two Low Energy Neutral particle Analyzers (LENA) at ASDEX. With the LENA devices /1/ the neutral charge exchange (CX)-flux from the Tokamak is mechanically chopped in bunches of 1 μs duration. After a flight path of ~2 m the time-of-flight (TOF) distributions are measured. These TOF distributions can be converted into energy distributions in the range of 10 eV/amu and to 1000 eV/amu. To obtain energy spectra with reasonable statistical relevance several hundred TOF distributions have to be summarized corresponding to 50 to 100 ms during an ASDEX discharge. Due to limited memory space, only 32 spectra can be acquired during one shot.

The differential CX-flux to the walls as measured with our analyzers is given by

$$\frac{d\Gamma}{dE} = \frac{E \cdot \sigma_{cx}(E)}{\pi (2m\pi)^{1/2}} \int_S dx\, n_o(x)\, n_i(x) \frac{e^{-E/T_i(x)}}{T_i(x)^{3/2}} \cdot \eta(x,E) \qquad (1)$$

$$\eta(x,E) = e^{-\int_S \sigma_{tot}(x,E)\,dx}$$

where x is the coordinate along the line of sight S, $n_i(x)$, $n_o(x)$ are the ion and neutral atom densities, $T_i(x)$, the ion temperature (in eV), and $\eta(x,E)$ the reabsorption of the neutrals /2/.

Apparently, the analyzer signal is a complicated function mainly of $n_o(x)$, $n_i(cx)$, and $T_i(x)$.

In many instances the total information of an energy spectrum is not required. For quick comparisons the consideration of integral quantities like the total neutral particle flux $\Gamma(cm^{-2}sec^{-1})$ and its mean energy $\overline{E}$ (eV) is sufficient and convenient. $\overline{E}$ contains information on the shapes of the spectra and is somehow connected to the ion temperature in the outer plasma regions. Also the total impurity production due to wall sputtering by these neutrals can be considered. For all integral quantities we have integrated over our energy range of $12.5 < E/M < 733$(eV/amu), i.e. 25 eV < 1470 eV for D_2 discharges. For the integration over the solid angle we assumed a cosine angular distribution. The latter is not quite correct as will be discussed later.

The integral quantities can be obtained directly from the experiment with high time resolution (up to a few ms during the shot) using the procedure described in Ref. 3. It is, however, not possible to retain the full information of the whole energy distribution from these data, once this

measuring mode was chosen. On the other hand, the integral quantities can always be obtained from the differential spectra, of course with the poor time resolution of this mode.

As the differential flux $d\Gamma(E)/dE$ decreases rapidly with increasing energy the total flux Γ measured with LENA comprises the majority of all neutrals impinging onto the wall. In Fig.1 the LENA data for an Ohmic discharge with $\overline{n}_e = 5.5 \cdot 10^{19}$ m^{-3} are shown together with data from the stripping neutral analyzer (NPA) located in the ONO sector. For this figure the NPA data were multiplied by a factor of 2.49 (adjustment at 500 eV). In the region of overlap there is good agreement of the spectra. In this case (high density) the flux for E > 1500 eV contributes only by less than 1 % to the total flux.

The first of the apparatuses, simply called "LENA" in the following, is located at the WSW sector of ASDEX. Its line of sight is horizontally and 12 cm below the midplane. In close proximity to the LENA is a movable auxiliary limiter. In the early phases (before ASDEX hardening) this was a mushroom limiter, which could be retracted to the vessel walls. Later it was a large carbon limiter, 50 cm high, concave in poloidal and convex in toroidal direction. (See Fig. 2). In its normal position it is at R = 211 cm (R major radius) i.e. 6 cm away from the magnetic separatrix in the midplane. At the tips of the limiter the distance is only 4.6 cm. After installation of this limiter the neutral flux Γ rose by a factor of ~ 20. Therefore the recycling of this limiter is the dominant gas source at this location.

The second apparatus, "LENA-S", is mounted in the SSO-sector of ASDEX. It is movable in a poloidal plane, with the pivot point 78 cm away from the separatrix in the midplane (s. Fig.3). Thus different lines of sight from perpendicular to $\vartheta = 60^o$ to the plasma surface are possible. Doing this, plasma regions with different temperatures and densities can be scanned. It was also intended to measure the angular distribution of the CX-neutrals leaving the plasma surface. However, as a change of the angle ϑ to the plasma surface (i.e. the separatrix) is always connected with different points of intersection with the plasma, when LENA-S is swivelled rather different sources of neutral gas are probed than the angular distribution. Most of the data are taken with $\vartheta = 0^o$.

It was impossible to operate both diagnostics at a time, because of the data acquisition system. Unfortunately, due to several vacuum accidents which included the failure of turbopumps and degrading of multipliers both LENA-S

were never available at the same time. Therefore we have no comparison for shots under really equal conditions.

2. Standard discharges

During the last experimental period "standard shots" were made with the following parameters: Ohmic heating, I_{pl}= 320 kA, B_t = 2.17 T (35 kA), $\bar{n}_e = 2{,}76 \cdot 10^{19}$ m^{-3} (20 fr). These shots were taken regularly at the beginning and end of each day and after major changes to document the status of the machine. Figure 4 shows the integrated flux Γ of D_2-standard shots as a function of the shot numbers. Apparently, there are large variations, up to a factor of 3. The flux is always large after a fresh boronization as indicated by the vertical lines. This has two reasons: 1) After boronization the walls contain large amounts of hydrogen (H_2). The recycling at the walls increases the H_2 content in D_2 discharges. This icreases the CX-flux Γ, since Γ is much larger for pure H_2 as compared for D_2 for equal discharges, as is discussed in § 8. 2) The discharges are very clean, i.e. the dilution of the working gas due to impurities is low. The lowest fluxes occur, when Z_{eff} is rather large. Moreover, the second and later standard shots on a day showed always more flux as the first one. This is shown in Fig. 5. At the same time the gas consumption decreased considerably. The external gas flux during the plateau phase (1.2 - 1.8 sec) decreases from 20.0 mbl/s = 4.8 10^{20} D_2-molecules/s to 10.7 mbl/s = $2.6 \cdot 10^{20}$ D_2/s. The second discharge is much cleaner as shows up in a considerably lower Z_{eff} /4/. In Table I the characteristic data fo the 1st and the 3rd shot (of this exp. day) are given:

#	Γ (10^{15})	Z_{eff} (r = 0)	Z_{eff} (r = 36)	n_D^+/n_e (r = o)	n_D^+/n_e (r =36)
(1) 30 824	0.95	2.1	4.7	0.82	0.38
(3) 30 826	1.29	1.88	3.8	0.85	0.53

Table 1

In the first shot (# 30824) Z_{eff} at the edge (r = 36) is especially high. Assuming a mean impurity Z_{imp}= 7 (CO) the dilution of the D^+ ion density n_D^+/n_e can be calculated. It is seen that $\Gamma^{(1)}/\Gamma^{(3)}$ = 1.37 and $(n_D^+/n_e)^{(1)}/(n_D^+/n_e)^{(3)}$

= 1.39 are almost equal. That means the dilution of the D^+ ion density - n_i in eq. (1) - alone should account for the lower Γ in the first shot. However, this effect should be even larger since the decrease of the external gas feed yields a much lower neutral gas density - n_o in equ. (1) - in the vicinity of the LENA-S, as is discussed in § 5. As the same line averaged density is obtained, more neutral gas most come from recycling sources, which are distributed over the whole torus.

3. Dependence on the plasma density

It has been shown in earlier papers /5/ that Γ increases almost linearly with increasing line averaged density, while $\overline{E}$ is decreasing. This is best seen in a shot where $\overline{n}_e$ is increased linearly up to the density limit. An example is shown in Fig. 6. In the uppermost figure is the line averaged density $\overline{n}_e$ as controlled by the gas valve (shown as GASV-S). $\overline{n}_e$ reaches a plateau value at $2.8 \cdot 10^{19} m^{-3}$ and is ramped up to the density limit at $5.8 \cdot 10^{19}\ m^{-3}$, where the current I_{pl} disrupts. Γ(center Fig.) follows almost exactly the trace of $\overline{n}_e$. $\overline{E}$ shows practically the opposite behavior.

This is also seen in Fig. 7 where the power flux P_n of the CX- neutrals is shown: Over a wide range of densities there is only a small variation of P_n. The power lost by the CX-neutrals is $P_n \sim 0.06\ W\ cm^{-2}$ i.e. ~ 15.6 kW, if this is integrated over the whole ASDEX plasma surface.

The close correlation of Γ and $\overline{n}_e$ as seen in Fig.6 holds only as long as the confinement type does not change. As shown earlier (Ref. 5, 6), Γ is decreasing considerably, for instance, when the Improved Ohmic Confinement (IOC) regime is reached. It was shown that

$$\Gamma \sim n_{es}\ \lambda_n$$

with n_{es} the density at the separatrix and λ_n the density decay length outside the separatrix, i.e. Γ scales with the particle content of the scrape off layer. This effect is plausible as the computer simulation of the neutral density (R. Schneider) shows clearly that the CX-particles observed with LENA originate from a shallow region at the plasma edge.

The energy spectra $d\Gamma/dE$ for 2 densities are shown in Fig.8. It is obvious that for the higher density the spectrum is much steeper and more curved in the log-plot than for the lower density case. This is also reflected in the decrease of the mean energy with increasing density. In the lower part of Fig. 8, the energy flux distribrutions for the same cases are shown.

4. Influence of I_{pl} and B_t

In discussing the influence of $\bar{n}_e$ it was assumed that other plasma parameters as I_{pl} and B_t were kept constant.

In Fig.9 the energy spectra for two discharges with high and low plasma currents I_{pl} are compared for 2 toroidal field strengths B_t. It is seen that the intensity as well as the shapes of the spectra depend strongly on I_{pl}. The differences are larger for higher B_t (bottom figure).

The differences of the integral quantities are summarized in table 2:

#	B_t (T)	I_{pl} (kA)	q_a	P_{OH} (kW)	Γ ($10^{15}cm^{-2}s^{-1}$)	$\bar{E}$ (eV)
28 345	2.18	448	2.35	555	1.32	242
28 349	2.18	271	3.26	303	1.31	239
28 350	2.78	448	3.02	403	1.42	320
28 351	2.78	271	4.97	264	1.60	207

Table 2

It is seen that Γ increases with increasing B_t, or at equal I_{plas} with q_a. The increase of $\bar{E}$ with I_{pl} can be attributed to the increase of the Ohmic heating power P_{OH}. There are, however, differences for different B_t values. In the Figs. 10 and 11 this behavior is shown for a series with I_{pl} variation in the range of 271 to 450 kA in smaller steps while B_t was kept at B_t = 2.18 T. In Fig. 10 Γ decreases nearly linearly with increasing P_{OH}. $\bar{E}$ increases with P_{OH}, but the slope of the curve becomes less steep at large I_{pl} values $\bar{E}$ is in a complicated manner connected to T_i in the edge region of the plasma. Thus the increase of $\bar{E}$ with P_{OH} reflects the increased heating. That $\bar{E}$ is not simply proportional to P_{OH} is plausible since the energy confinement time τ_E decreases from ~ 50 ms to ~ 30 ms in the range of I_{pl} discussed here.

Unfortunately, we have no data for a series, where B_t was varied while I_{pl} was kept constant.

5. Influence of the external gas valve

The neutral fluxes measured with LENA (in the WSW sector) are not dependent on the location of the external gas valve. (This valve was never very close to the LENA location). This is understood because the neutral gas density at this location is dominated by the recycling at the nearby protection limiter.

This is different for the LENA-S system, which is not influenced by nearby limiting structures. The normal location of the controlled gas valve is in the S sector ~ 1 m away from LENA-S. Figure 12 shows two standard shots with the gas valve in the S and in the ONO-sector. It is seen that not only $d\Gamma/dE$ is considerably lower for the ONO gas valve, but also the shape of the curves, i.e. $\bar{E}$ is different. For comparison data for a standard shot measured with LENA(WNW) are added in the last column.

shot no.	28303	28 302	23 847
location of GASV	ONO	S	LENA(WNW)
$\Gamma(10^{15}cm^{-2}s^{-1})$	0.58·	1.05·	7.5·
E (eV)	370	408	365

Table 3

A number of shots in which $\bar{n}_e$ was ramped up were taken for different locations of the controlled gas valve. In Table 4 the gas feed came through the valve in the S(normal), through the upper divertor chamber (Div.), through the 4 valves which are normally being used for the plasma startup gas, and through a valve in the East at the inner wall of ASDEX.

The data are given for 2 densities (2.8 and $4.1 \cdot 10^{19}$ m^{-3}). In the last column, the Γ data are related to the value with the normal valve (S).

It is obvious that the fluxes depend largely on the gas valve location. The effect is larger for higher densities.

It has already been shown by Wagner /7/ that the neutral density around a source has a decay length of ~ 40 cm. Therefore, ~ 8% of the additional neutral density n_o in the vicinity of the gas valve is still present at the

LENA-S location giving an enhancement in n_o here. n_o(LENA-S) would be larger by a factor of 8 as compared to the averaged value for the whole torus, if the external gas feed would be the only source for n_o. There are, of course, other sources as recycling for wall structures and refuelling from the divertor.

#	GASV	$\bar{n}_e(10^{19}m^{-3})$	$\Gamma(10^{15}cm^{-2}s^{-1})$	$\bar{E}$(eV)	Γ/Γ_S
26 563	S	2.8 4.1	0.609 1.12	274 164	1 1
26 575	upper Div.	2.8 4.1	0.445 0.746	270 207	0.73 0.67
26 567	start up valves	2.8 4.1	0.242 0.395	236 207	0.41 0.35
26 569	East inner wall	2.8 4.10	0.33 0.53		0.54 0.47

Table 4

For the determination of transport coefficients gas oscillation experiments by a sinuidal variation of the voltage at the gas valves have been performed. An example is shown in Fig. 13: In the uppermost picture the line averaged density through a line of sight intersecting the plasma 30 cm from its center (i.e. this monitors the density in an edge region) together with the divertor density as measured with the microwave inferometer are depicted. At 2s neutral injection starts. In the center figure the neutral flux Γ (measured with LENA-S) and in the lowest figure its mean energy $\bar{E}$ are shown. It is seen that Γ varies in phase with $\bar{n}_e$ and n_{eD}, while $\bar{E}$ varies in the opposite manner. It is remarkable that the relative amplitudes of the oscillations of n_{eD} and Γ are almost equal. This would again support the earlier finding that Γ reflects variations of n_i in the SOL (scrape off layer). We know, however, that there is also a variation of n_o in this region. The variation of $\bar{E}$ reflects the cooling of the edge region by the gas puff.

Another example for gas puff variations are shown in Fig. 14. In this case the discharge went into the IOC mode in the time interval 0.9 - 1.5s. (After 1.5s the plasma was shifted inward). During this time the external gas

puff (GASV) was slightly varied (much smaller amplitudes than in Fig. 13). There are no alterations of the flux Γ but large variations of $\overline{E}$.

A curious case is shown in Fig. 15. Large sinuidal oscillations of the gas valve (GASV) caused a slow rise of $\overline{n}_e$. H_4 ($\overline{n}_e$ at r = 0.75 a), D_α-light emission in the X-point region, the snifferprobe signal, and the divertor density n_{eD} all show the corresponding variations. For Γ the variation is hardly visible before a certain event at 1.3s and is more obvious after that event. The divertor electron temperature, T_{eD}, and the mean neutral energy, E_{mean}, show large variations before 1.3s which are no longer visible after 1.3s. The only effect, which we are aware of, is that an increasing MHD-activity starts at 1.3s.

Not in all cases are the variations in Γ and $\overline{E}$ directly visible especially at higher frequencies of the gas puff oscillations. In Fig. 16 the neutral flux Γ, the voltage at the gas valve, $\overline{E}$, and the signal of the outermost channel of the Li-beam diagnostic, K_{10} (n_e in the scrape off layer) are shown. On first sight there are no obvious correlations between these signals. Existent correlations become visible if the cross-correlation functions $\phi(\tau) = C \int_T x(t) \cdot y(t + \tau)dt$ are discussed, where x(t) and y(t) are the signals in question. Fig. 17 shows the cross correlation functions of Γ with K_{10} and of $\overline{E}$ with H_4, respectively. This shows clearly the correlation of Γ with the SOL-density and the counter correlation of $\overline{E}$ with H_4.

6. Pellet Injection

Another way of refuelling the plasma is by pellet injection. The LENA signals show a strong response to the injection of the pellets especially at low densities. Fig. 18 shows a shot where slow (200 m/s) D_2-pellets were injected in a low density discharge ($\overline{n}_e = 1.38\ 10^{19} m^{-3}$). In the lowest trace (FD, arbitrary units,) a photodiode signal is shown, which indicates the injection times. Γ shows large and sudden excursions upon pellet injection. $\overline{E}$ drops immediately and recovers slowly. This indicates the sudden cooling of the edge by the pellets.

This figure is an example for the time resolution (1.8 ms in this case) available with LENA when the integral measuring mode is used.

7. Influence of the plasma position

In ASDEX the plasma can be shifted up and down ($\Delta Z \neq 0$). The plasma can also be shifted inward and outward which means a variation of the major plasma radius between 163 cm < R_{pl} < 168 cm, R_{pl} = 165 being the normal position. These shifts cause different reactions of the neutral fluxes measured with the LENA at different locations:

With LENA (close to the auxiliary limiter) a large increase of Γ is observed when the plasma is shifted outward. The same is true when the limiter is moved towards the plasma as shown in Table 5 for a series of standard shots.

#	R_L	R_{pl}	$\Gamma(10^{15})$	E(eV)	Δ_{LS}
24 577	211	165	5.1	370	6 cm
24 578	211	167	9.4	490	4 cm
24 580	209	167	21.0	570	2 cm
24 582	209	165	12.6	485	4 cm

Table 5

R_L Limiter position measured in the midplane (s. fig. 1)

R_{pl} Major plasma radius

Δ_{LS} Distance separatrix - limiter (in the midplane)

Also, E_{mean} increases when the distance between separatrix and limiter Δ_{LS} is decreased. The large flux increase with decreasing Δ_{LS} is easily understood with the increase of the recycling at the limiter which increases the neutral density. The plasma ion flux density along field lines is

$$J^+ = 1/2\ n_i\ C_s(T_i, T_e) \qquad (2)$$

where C_s is the ion acoustic speed /8/. Assuming the usual decay length λ = 1.5 cm for $n_{e,i}$ and $T_{e,i}$ outside the separatrix the integration over the limiter contour (s. Fig. 2) yields

$$J^+_{(1)} = 4.93 \cdot 10^{18}\ cm^{-2}s^{-1} \quad \text{for} \quad \Delta_{LS} = 6\ cm\ (normal)$$

$$J^+_{(2)} = 3.15 \cdot 10^{19}\ cm^{-2}s^{-1} \quad \text{for} \quad \Delta_{LS} = 4\ cm,$$

i.e. an increase by a factor of 6.4 while the observed flux Γ increases only by a factor of ~ 2.5.

Apparently, the absorption factor $\eta(E,x)$ in equ. (1) increases so that Γ does not increase as much as the ion flux onto the limiter. This is coroborated by the observed increase of $\overline{E}$. This is due to the preferential absorption of the low energy particles.

It is seen from Table 5 that moving the plasma toward the limiter increases Γ less than moving the limiter to the plasma. This may be due to the fact that in the first case other structures in the ASDEX vessel which take up ion flux can become important in reducing the flux onto the limiter.

Γ in LENA is also sensitive to up-down shifts. When $\Delta Z>0$ Γ decreases, because the LENA line-of-sight is 12 cm below the midplane. The main recycling responsible for the LENA flux occurs at the lower limiter tip which is reduced when the plasma is shifted upwards.

The conditions are quite different for LENA-S where no limiting structure is nearby. In Fig.19 $d\Gamma/dE$ for 3 standard shots with different plasma radii are shown. The flux decreases with increasing R_{pl}, but also the shapes of the curves change. The integrated flux Γ together with the divertor pressures (DMO and DMU) is shown in Fig. 20. As in many other cases, the divertor pressure is closely connected to the neutral flux Γ (see Ref. 5). It is interesting that the gas consumption in all cases when $R_{pl} \neq 165$ is lower as compared to the case when the plasma is in its normal position at R_{pl} = 165 cm. Apparently, the plasma flux in the scrape-off-layer which is guided into the divertor is partly falling onto the edges of the divertor throat where it recycles. Thus less gas from the external gas feed is needed. Nevertheless, is the divertor chamber pressure decreasing as Γ decreases when the plasma is shifted outwards.

The same effect is illustrated by Fig. 21. The line averaged density $\overline{n}_e$ was programmed to three plateau values for the two shots with R_{pl} = 165 and 167. During the second and third plateaus both discharges went into the IOC regime, which is characterized by a substantial drop in the CX-flux. In the lower part of Fig. 21 the integrated flux Γ for the 2 plasma radii is shown. At all times Γ for R_{pl} = 167 is only 0.75 times that for R_{pl} = 165 (normal position).

A possible explanation for this behavior is the following: The external gas flux hits the plasma surface at an estimated area of ~ 1/4 m^2. The gas is being ionized, but a part of the ions is reneutralized by charge exchange and can return to the wall. The plasma has a kind of albedo $0.5<A<0.8$ for the neutral gas /9/. At the walls it is reflected at A ~ 1 and again partly from the plasma. This chain of reflection processes governs the lateral distribution of the neutral density at a distance from the gas valve. It is plausible that

the distance d_{pw} between plasma and material wall is a critical quantity in this context. From Wagner's experiments /6/ the neutral density in a distance x from the gas source has the form

$$n_o \sim e^{-x/\lambda} \quad , \text{ where } \lambda \sim d_{pw}.$$

Thus, the influence of the gas inlet on the LENA-S-fluxes should decrease with decreasing d_{pw}, i.e. with increasing R_{pl} /10/. A quantitative verification of this ideas would require a detailed computer simulation.

When LENA-S is in its normal position (line of sight horizontally in the midplane, $\alpha = 0$, see Fig. 3) there is no variation of Γ or $\overline{E}$ with a vertical plasma shift (nor should a variation be expected). However, when LENA-S is swivelled to $\alpha = 28^o$ with the line of sight to the lower plasma edge, Γ depends largely on the vertical plasma position ΔZ as is shown in Fig. 21. When the plasma is shifted up- or downwards from the centre ($\Delta Z \neq 0$) the magnetic configuration alters such that there is a connection between the inner and outer side of the scrape-off-layer. Only a small part of the ion flux penetrating the separatrix is guided into the lower divertor when the plasma is shifted upwards ($\Delta Z > 0$) and vice versa.

During the time when these data were taken, the lower divertor bypasses were still open, while the correponding upper bypasses were closed, i.e. the refuelling from the lower divertor was especially large. This shows up also in the external gas feed required to maintain the preprogrammed density. Due to the refuelling from the lower divertor almost no external gas feed is required for $\Delta Z < 0$, while a significant gas feed is necessary for the upper divertor case. It is obvious from Fig. 22 that the neutral flux Γ decreases stepwise when the plasma is shifted upwards. The slow decrease of Γ for $\Delta Z > 1$ is connected with a decrase of $\overline{E}$ from $\overline{E}$ = 200 eV at $\Delta Z = +1$ to $\overline{E}$ = 130 eV at $\Delta Z = +3$. Γ decreases because the LENA line of sight intersects a smaller plasma area with upward shifting and E decreases, because the probed plasma area shifts to the edge.

8. Isotope effects

The LENA measuring principle does not allow the distinction of particles with different masses. Only the quantity E/M is measured. Therefore, spectra measured with the gas mixture are hard to interpret. After changing the discharge gas it takes a large number of shots before the dominant ion species is from the new gas.

In general, is the flux Γ for Hydrogen discharges much larger than for corresponding Deuterium shots. In Table 6 the first two standard shots of a "Hydrogen" and a "Deuterium day" are compared. The walls were boronized. According to the divertor mass spectrometers the working gas contains ~ 25 % of the other isotope in each of these shots.

	#	$\Gamma(10^{15}cm^{-2}s^{-1})$	$E_{mean}(eV)$
H_2	30866	1 48	168
	30867	1.75	161
D_2	30931	0.94	340
	30932	1.16	325

Table 6

For the comparison of H_2 and D_2 discharges we integrated over the same energy interval 245 eV to 735 eV rather than over the entire accessible interval of E/M as in all other cases discussed in this report. Therefore the values of Γ and E_{mean} are slightly smaller.

In this case is $\Gamma(H_2) \sim 1.5\ T(D_2)$. The differences of $\Gamma(H_2)$ and $\Gamma(D_2)$ are even larger for steel walls of ASDEX.

It is remarkably that the mean energy for H_2 is much lower than for D_2. This shows up in the different shapes of the energy distribution dT/dE for the two isotopes as shown in Fig. 23.

The isotope effect observed with LENA shows up also in other edge properties: the electron density at the separatrix, for instance, is $n_{es}(H_2) = 1.5\ n_{es}(D_2)$ in the example discussed by Bessenrodt-Weberpals /11/. The correlation of Γ with n_{es} was discussed already in § 3.

9. Sawtooth-free discharges

Sometimes sawtooth-free discharges ocurred spontaneously in ASDEX. These discharges are characterized by improved energy and particle confinement connected with peaked density profiles. Also the LENA signals show remarkable

differences. In Fig. 24 the spectra $d\Gamma/dE$ are compared for the Ohmic and NI heated phases for a sawtoothing and sawtooth-free discharge. In both cases the curves are lower in the sawtooth-free case. This is again reflecting the fact that Γ depends on the density at the edge, which is reduced due to the peaking of the density profile.

10. Conclusion

A large amount of data on the low energy CX fluxes have been accumulated during the operational period of ASDEX. Some of them were presented in earlier publications /3,5,6/. In this report some typical ohmic discharges have been chosen to illustrate the experimental findings.

The discussion of LENA fluxes and mean energies together with other edge quantities measured at ASDEX give a consistent picture. They deliver, however, only a little contribution to the understanding of ASDEX or the divertor tokamak principle. The consideration of the LENA observations discussed in this report is, however, necessary when the LENA specific quantities like impurity production at the walls and edge ion temperatures are determined. With eleborated computer simulations of the neutral gas (EIRENE code) ion temperatures profiles in the outer plasma region can be determined from the LENA-spectra. This will be discussed in a forthcoming paper /12/.

References

/1/ H. Verbeek, J. Phys. E (Scient. Instr.). 19 (1986) 964.

/2/ F. Wagner, J. Vac. Sci. Technol. 20 (1982) 1211

/3/ V. Dose, H. Verbeek, Appl. Phys. Lett. 51 (1987) 229

/4/ K.H. Steuer, Europhys. Conf. Abstr. 12B (1988) 31.

/5/ H. Verbeek et. al. J. Nucl. Mat. 162-164(1989) 557.

/6/ H. Verbeek, W. Poschenrieder et al., Plasma Phys. Contr. Fus. 32(1990) 651

/7/ F. Wagner: Report IPP III/71 (1981)

/8/ P.C. Stangeby in Physics of Plasma Wall Interactions in Controlled Fusion, Eds. D.E. Post, R. Behrisch, New York, London (1984).

/9/ S. Rehker, H. Wobig, Plasma Phys. 15 (1973) 1083

/10/ J. Neuhauser, private communication

/11/ M. Bessenrodt-Weberpals et al., Proc. 9th PSI, 1990, to be published in J. of Nucl. Mater.

/12/ R. Schneider, H. Verbeek, J. Neuhauser, Proc. EPS-Conference on Controlled Fusion and Plasma Physics, Berlin 1991.

Figure Captions

Fig. 1: CX neutral energy distribution measured with LENA (...) and the stripping analyzer NPA (xxx).

Fig. 2: Auxiliary limiter in the WSW sector of ASDEX.

Fig. 3: Schematic of the geometry of LENA-S.

Fig. 4: The integrated flux Γ of CX-neutrals in all Deuterium standard shots measured with LENA-S as a function of the ASDEX shot number.

Fig. 5: The first and the second standard shot of the 640th day:
Upper Fig.: Voltage at the external gas valve (GASV, a.u.) and the integrated gas consumption (QGAS D_2).

Lower Figure: The neutral flux Γ averaged over 100 ms.

Fig. 6: A "standard density limit shot".
Upper Fig.: Plasma current, line averaged density $\bar{n}_e$ and voltage at the gas valve (GASV-S). Centre Fig.: CX-neutral flux Γ. Lower Fig.: mean energy of the neutrals.

Fig. 7: The power transported by the CX-neutrals during the shot of Fig. 6.

Fig. 8: Particle flux distribution $d\Gamma/dE$ ("Flux", $D^o/cm^2 \cdot s \cdot eV \cdot sr$) and energy flux distribution dP/dE ("EFLUX", $W/cm^2\ eV \cdot sr$) for $\bar{n}_e = 5.5 \cdot 10^{19} m^{-3}$ (solid curve) and $\bar{n}_e = 2.8 \cdot 10^{19} m^{-3}$ (dashed curves) from the ohmic discharge of Fig. 6.

Fig. 9: $d\Gamma/dE$ ("Flux", $D^o/cm^2 s \cdot eV \cdot sr$) for J_{pl} =271 kA and 448 kA for B_t=2.18 T (upper Fig.) and B_t = 2.78 T (lower Fig.).

Fig.10: The CX-flux Γ as a function of the Ohmic heating power.

Fig.11: Mean energy of the CX-neutrals vs. Ohmic heating power.

Fig.12: $d\Gamma/dE$ for location of the external gas valve in the S and ONO sectors of ASDEX.

Fig.13: Gas oscillations. Upper Fig.: line averaged densities in the edge of the main chamber $n_e(0.75\ a)$ and in the divertor chamber n_{eD}; Centre Fig.: CX-flux Γ; Lower Fig.: E_{mean} of CX-neutrals. At 2 s is the onset of the neutral injection heating.

Fig.14: Gas oscillations during and IOC-shot.
The CX-Flux Γ (uppermost trace), its mean energy $\bar{E}$, and the voltage at the controlled gas valve (GASV). (At 1.5 s the plasma was shifted inward to R_{pl} = 162.5 cm).

Fig.15: Various signals during a shot with gas oscillations
(see text for details).

Fig.16: Gas oscillations. CX-Flux Γ, voltage at the gas valve (GASV), $\bar{E}$ of CX-neutrals, and signal K10 of the outermost channel of the Li-beam diagnostic.

Fig.17: Cross correlation functions of a) Γ with K10 and b) $\bar{E}$ with $\bar{n}_e(0.75\ a)$ for the shot of Fig.16.

Fig.18: Response of the CX-flux Γ (upper trace), its mean energy E_{mean} (centre) on the injection of small D_2 pellets. The injection times are indicated by the spikes in the FD-signal (lowest trace).

Fig.19: $d\Gamma/dE$ for standard discharges with different plasma major radii R. (LENA-S).

Fig.20: CX-Flux Γ, and pressures in upper (DMO) and lower (DMU) divertor chambers vs. major plasma radius R_{pl}.

Fig.21: In both shots # 25730 and # 25732 were J_{pl} and $\overline{n}_e$ as in the upper figure. The lower Fig. shows Γ for 2 plasma radii R_{pl}.

Fig.22: Γ as measured with LENA-S in its lowest position ($\alpha = 28^o$, see fig. 3) vs vertical plasma shift. In the upper part the pressure in the upper (DMO) and lower (DMU) divertor chambers and the gas puff rate are given.

Fig. 23: Comparison of the CX energy distributions for standard H_2 and D_2 discharges.

Fig.24: Comparison of $d\Gamma/dE$ for # 28826 (sawtooth-free)with # 28827 (with sawteeth) for the Ohmic (upper fig.) and NI heated (lower fig.) phases.

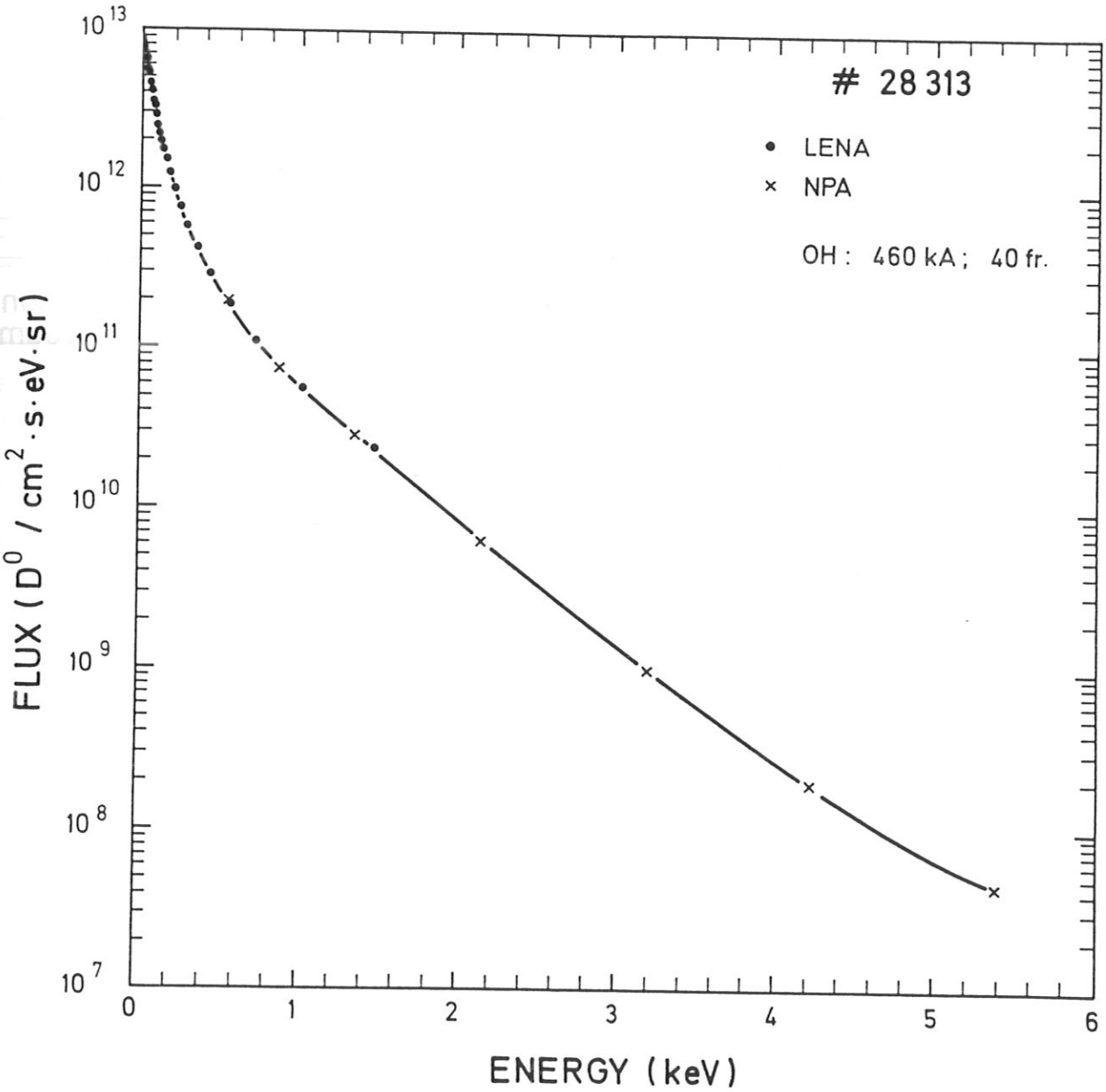

Fig.1: CX neutral energy distribution measured with LENA (...) and the stripping analyzer NPA (xxx).

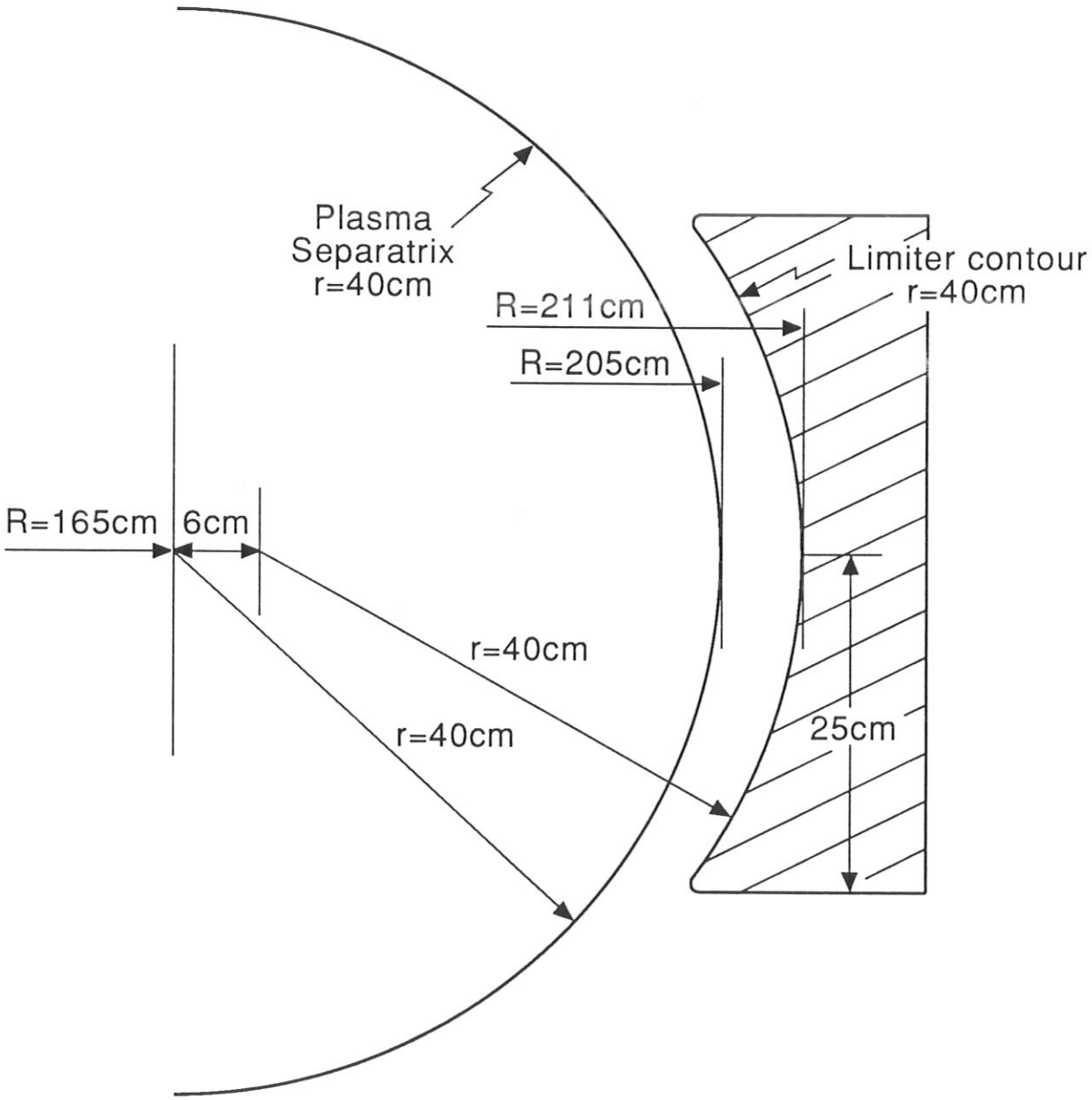

Fig.2: Auxiliary limiter in the WSW sector of ASDEX.

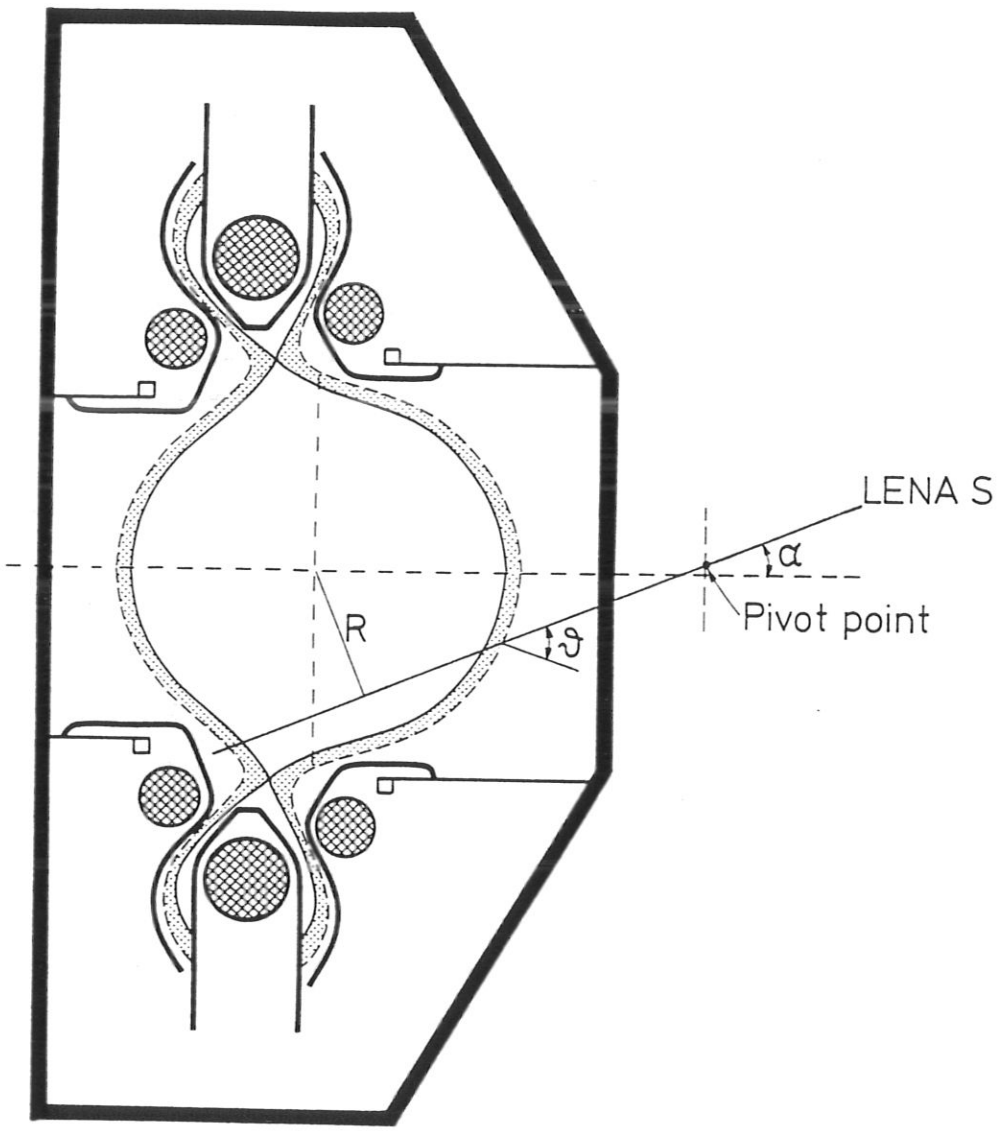

Fig.3: Schematic of the geometry of LENA-S.

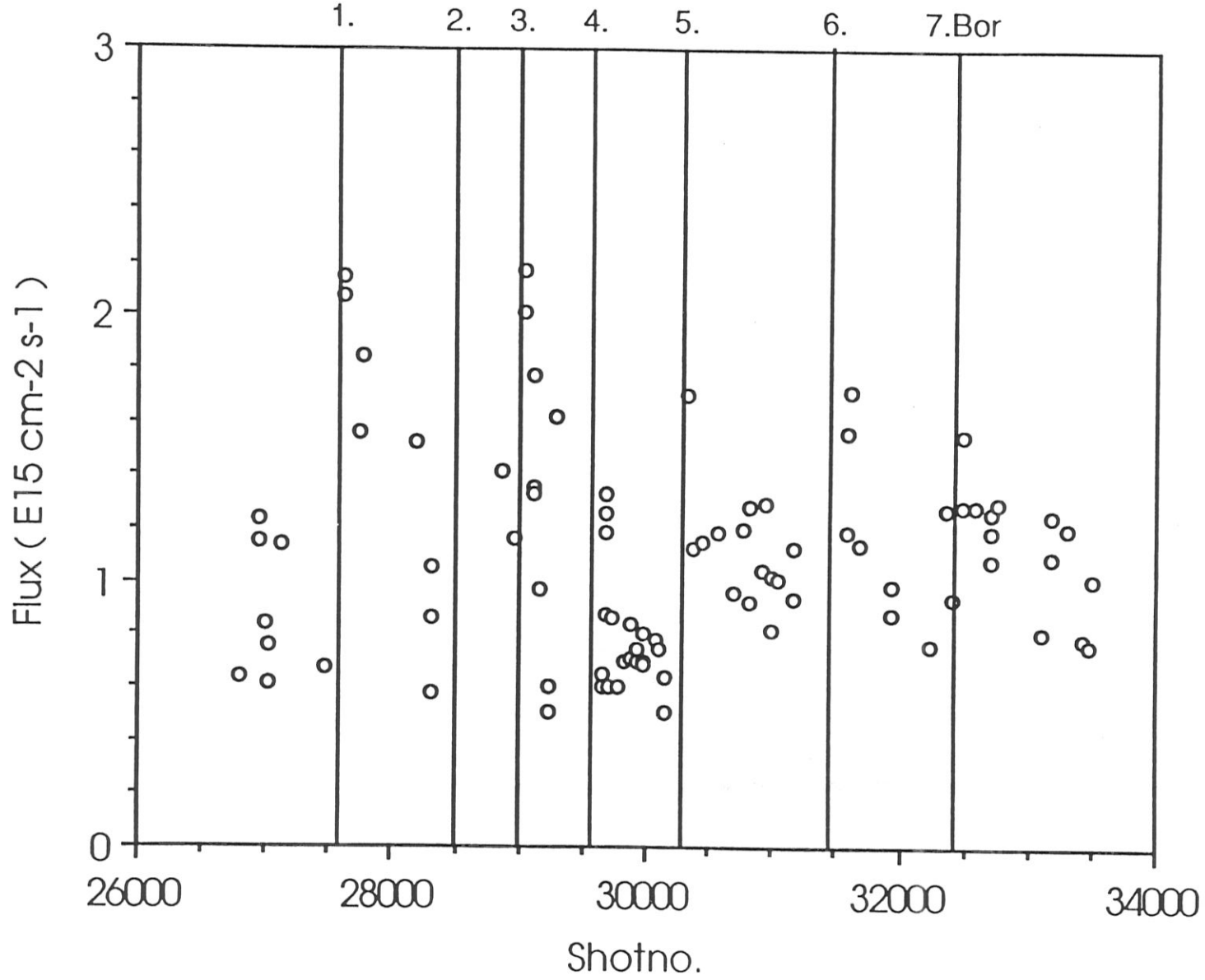

Fig.4: The integrated flux Γ of CX-neutrals in all Deuterium standard shots measured with LENA-S as a function of the ASDEX shot number.

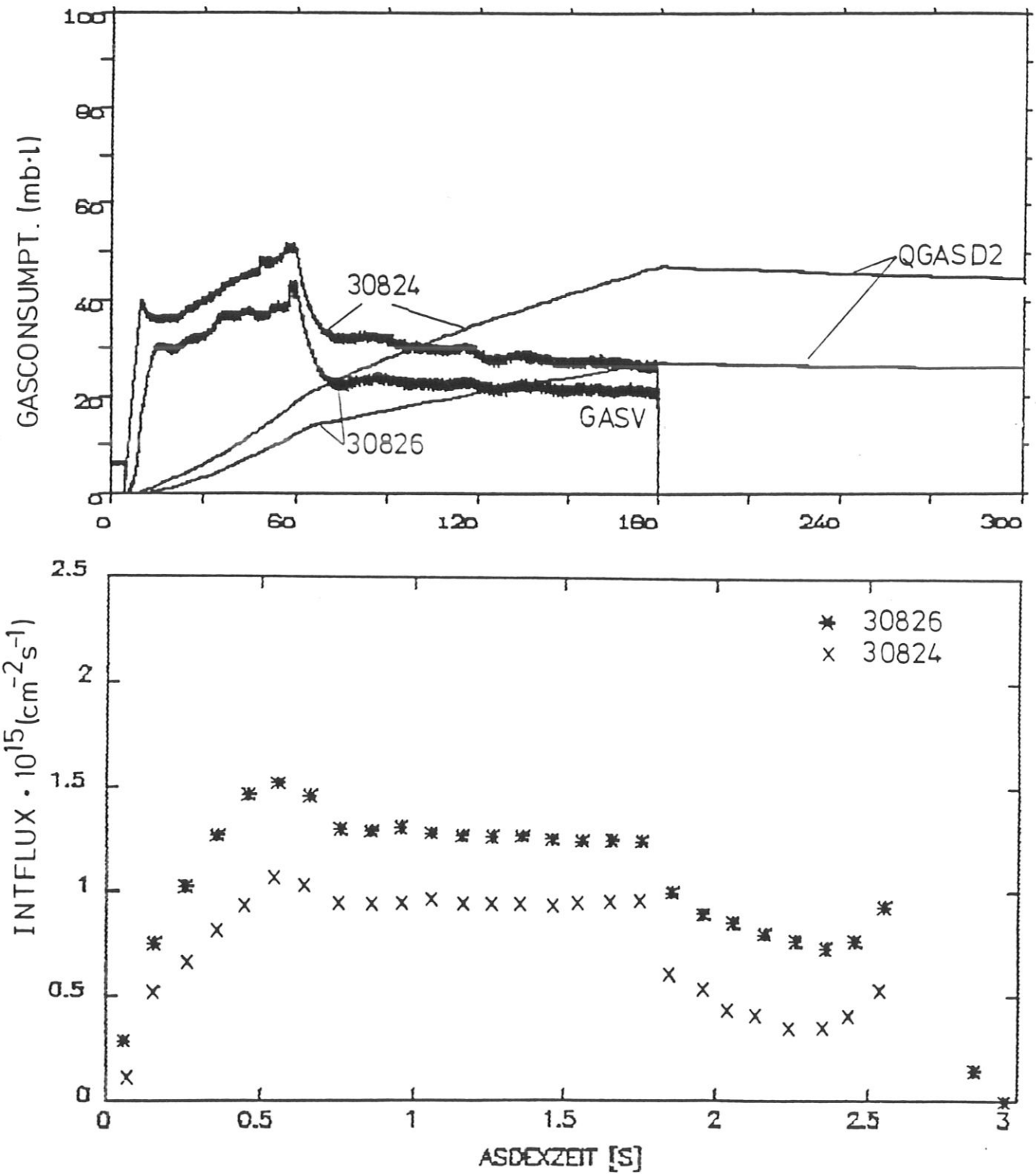

Fig.5: The first and the second standard shot of the 640th day:
Upper Fig.: Voltage at the external gas valve (GASV, a.u.) and the integrated gas consumption (QGAS D_2).
Lower Figure: The neutral flux Γ averaged over 100 ms.

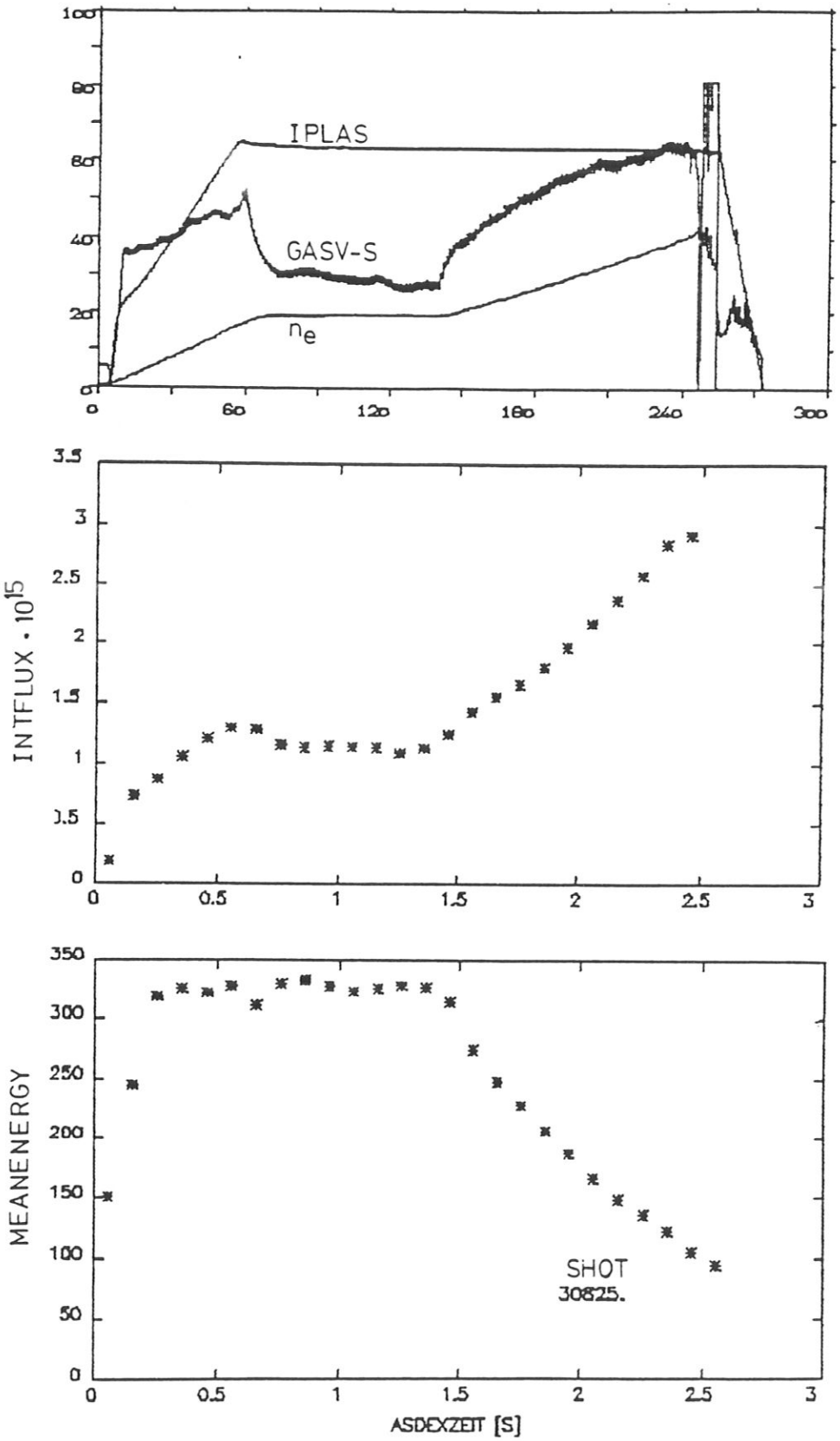

Fig.6: A "standard density limit shot".
Upper Fig.: Plasma current, line averaged density $\bar{n}_e$ and voltage at the gas valve (GASV-S). Centre Fig.: CX-neutral flux Γ. Lower Fig.: mean energy of the neutrals.

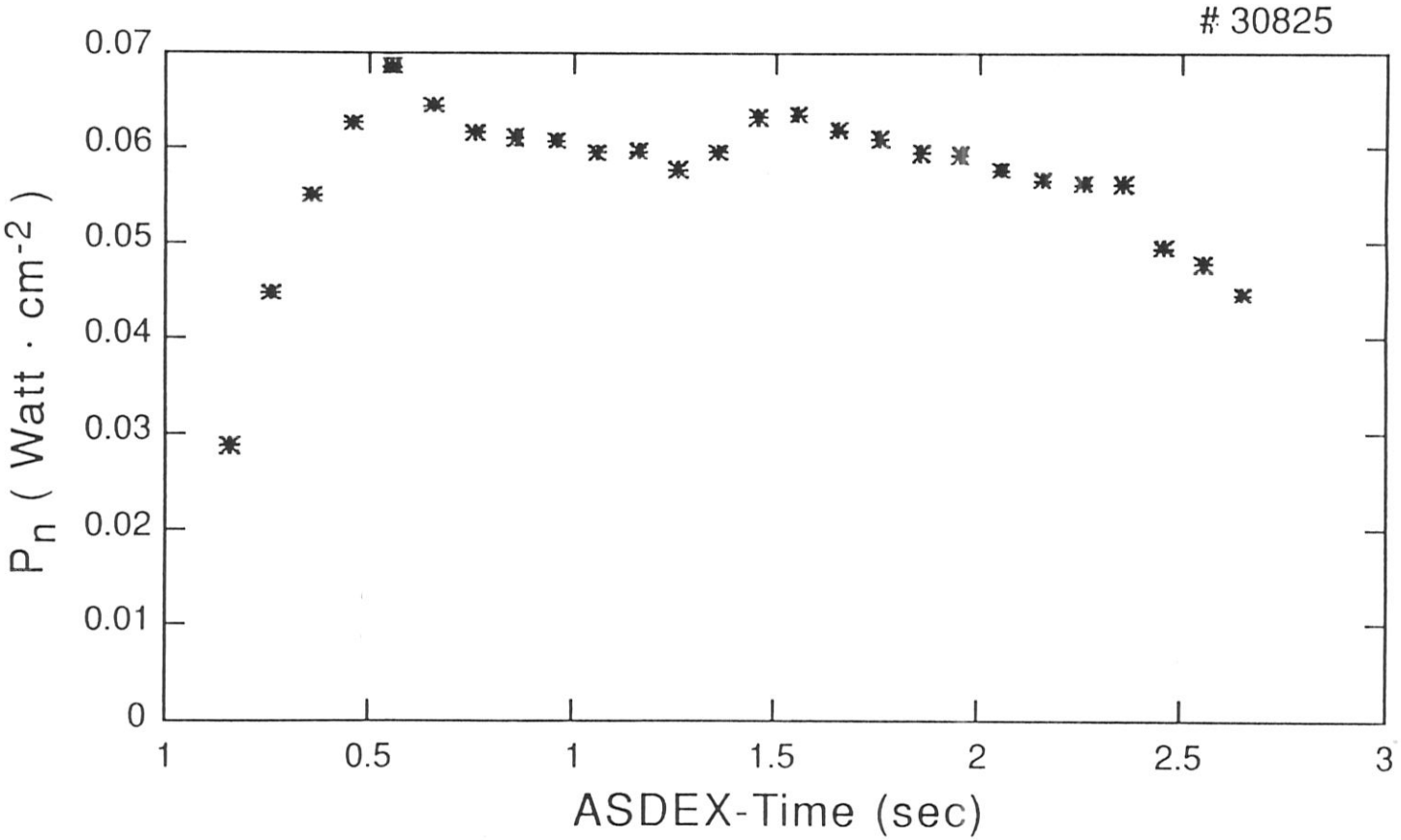

Fig. 7: The power transported by the CX-neutrals during the shot of Fig. 6.

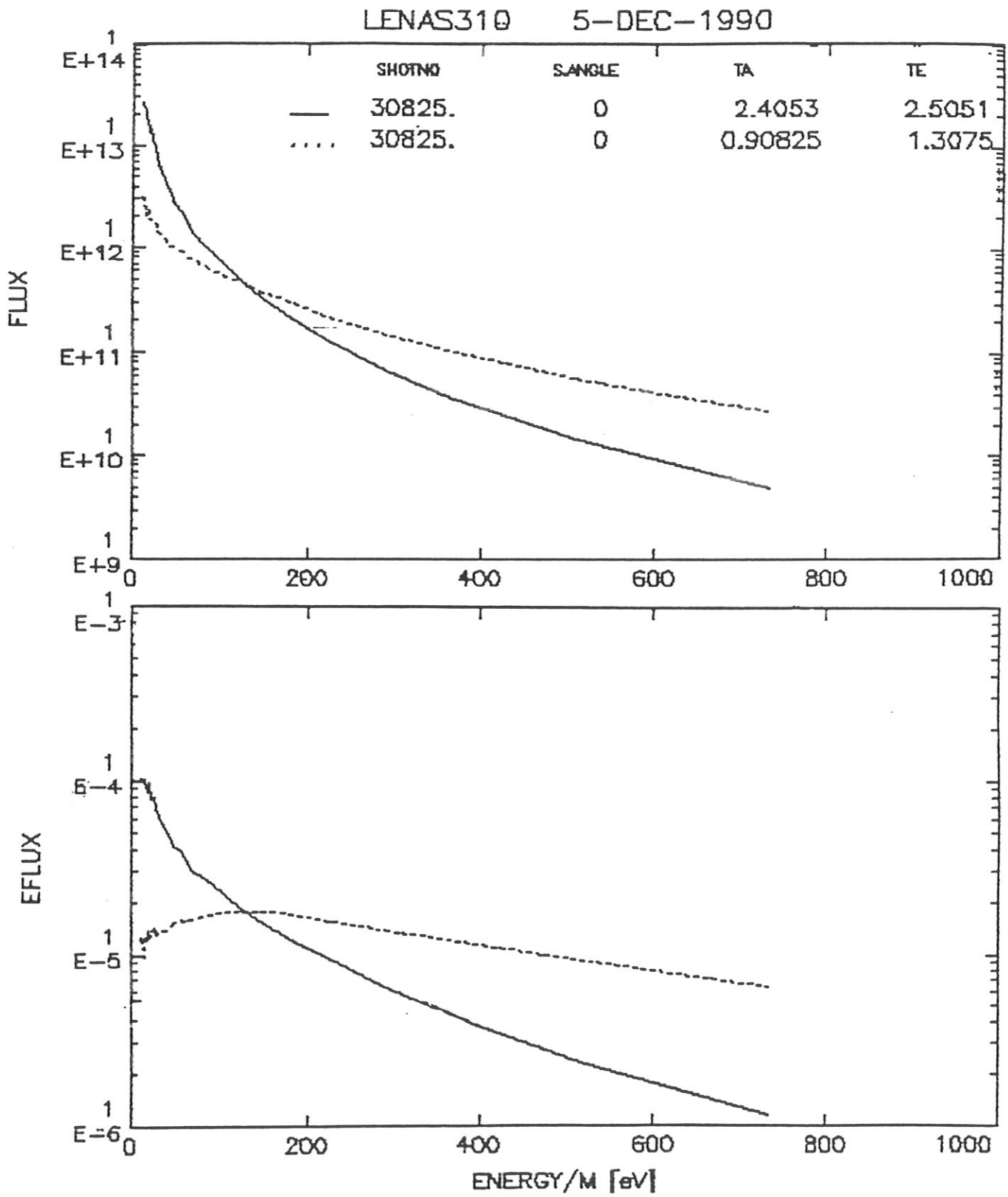

Fig.8: Particle flux distribution $d\Gamma/dE$ ("Flux", $D^o/cm^2 \cdot s \cdot eV \cdot sr$) and energy flux distribution dP/dE ("EFLUX", $W/cm^2 \cdot eV \cdot \cdot sr$) for $\overline{n}_e = 5.5 \cdot 10^{19} m^{-3}$ (solid curve) and $\overline{n}_e = 2.8 \cdot 10^{19} m^{-3}$ (dashed curves) from the ohmic discharge of Fig. 6.

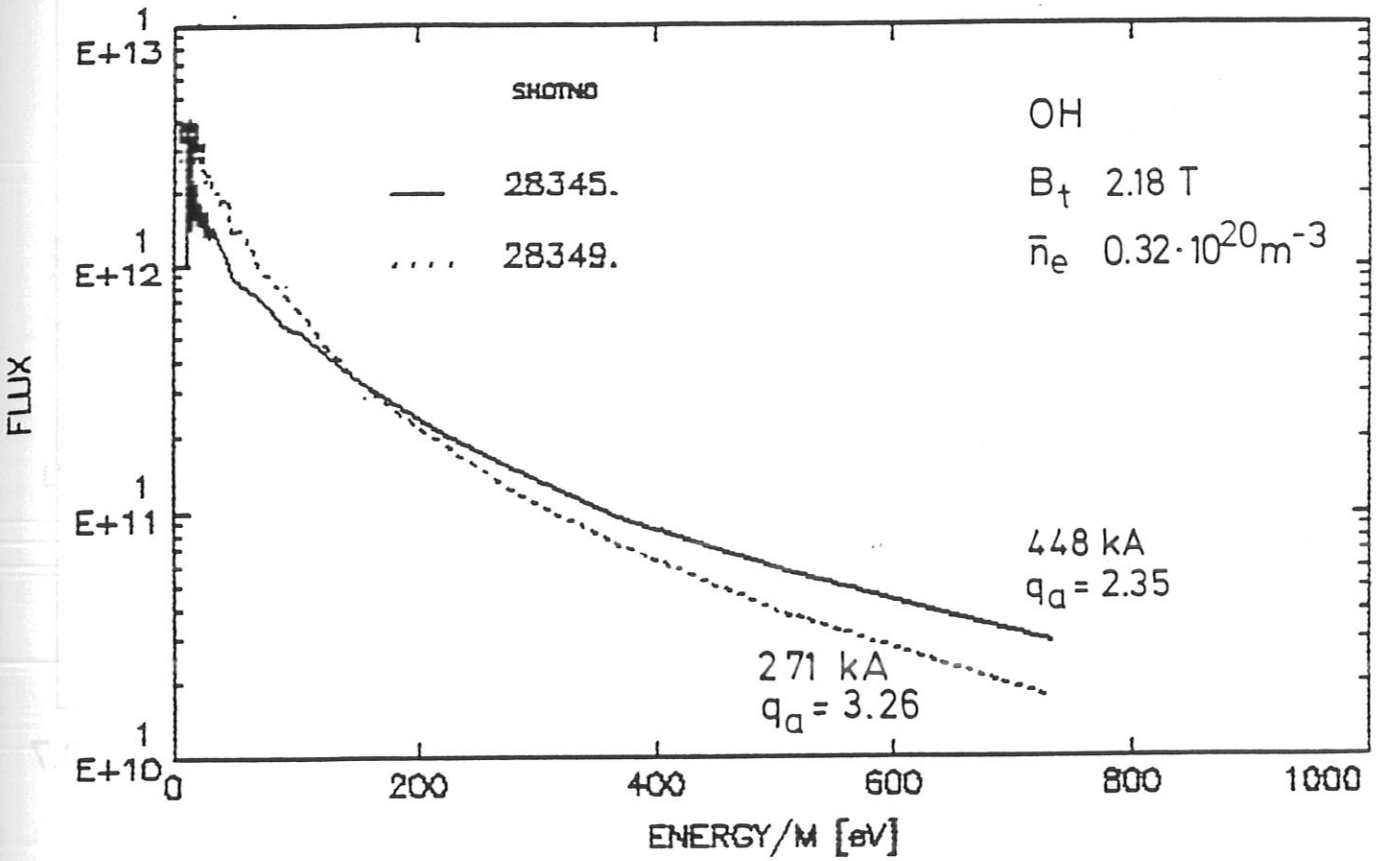

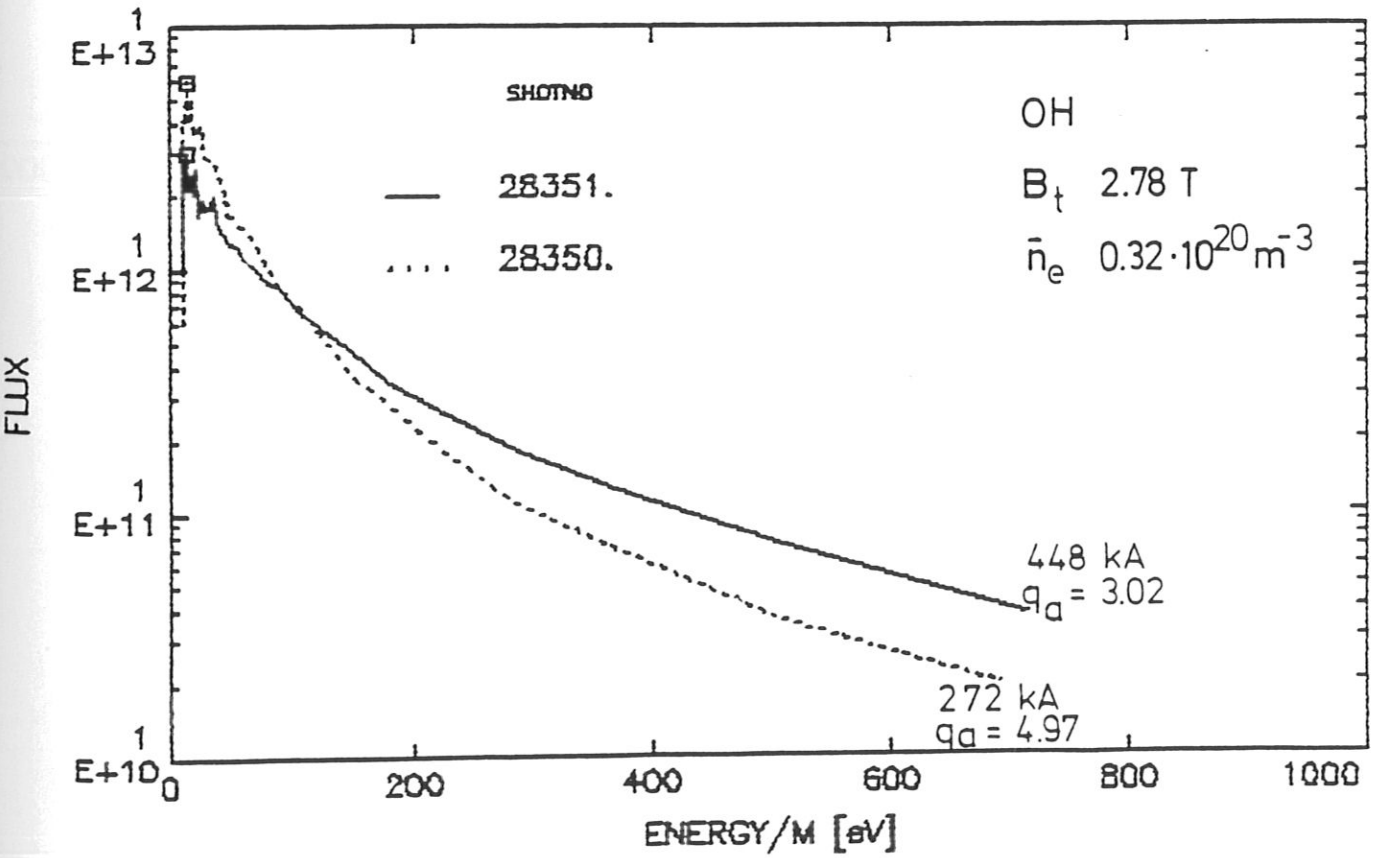

Fig.9: $d\Gamma/dE$ ("Flux", D^o/cm^2s eV sr) for J_{pl} =271 kA and 448 kA for B_t = 2.18 T (upper Fig.) and B_t = 2.78 T (lower Fig.).

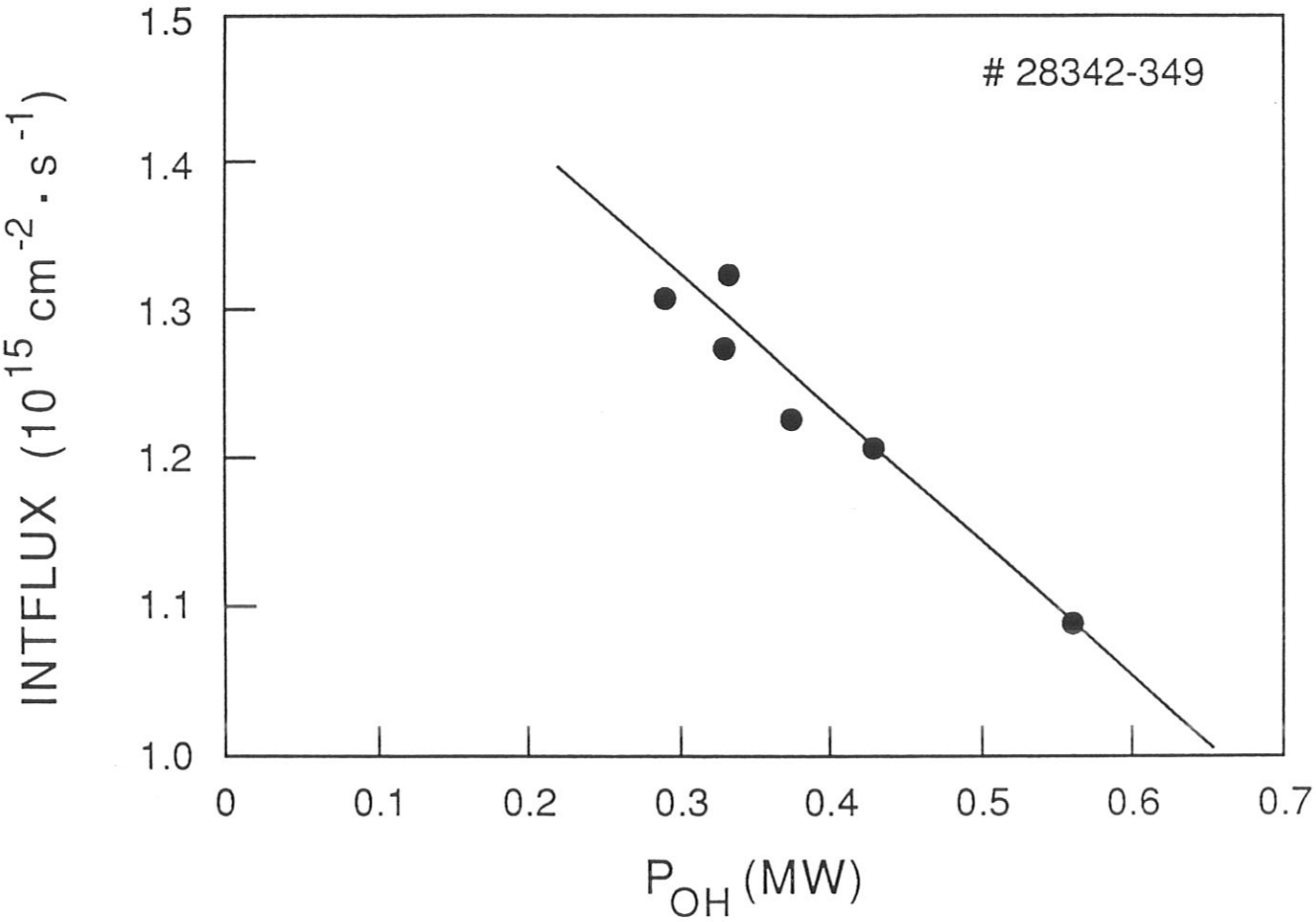

Fig.10: The CX-flux Γ as a function of the Ohmic heating power.

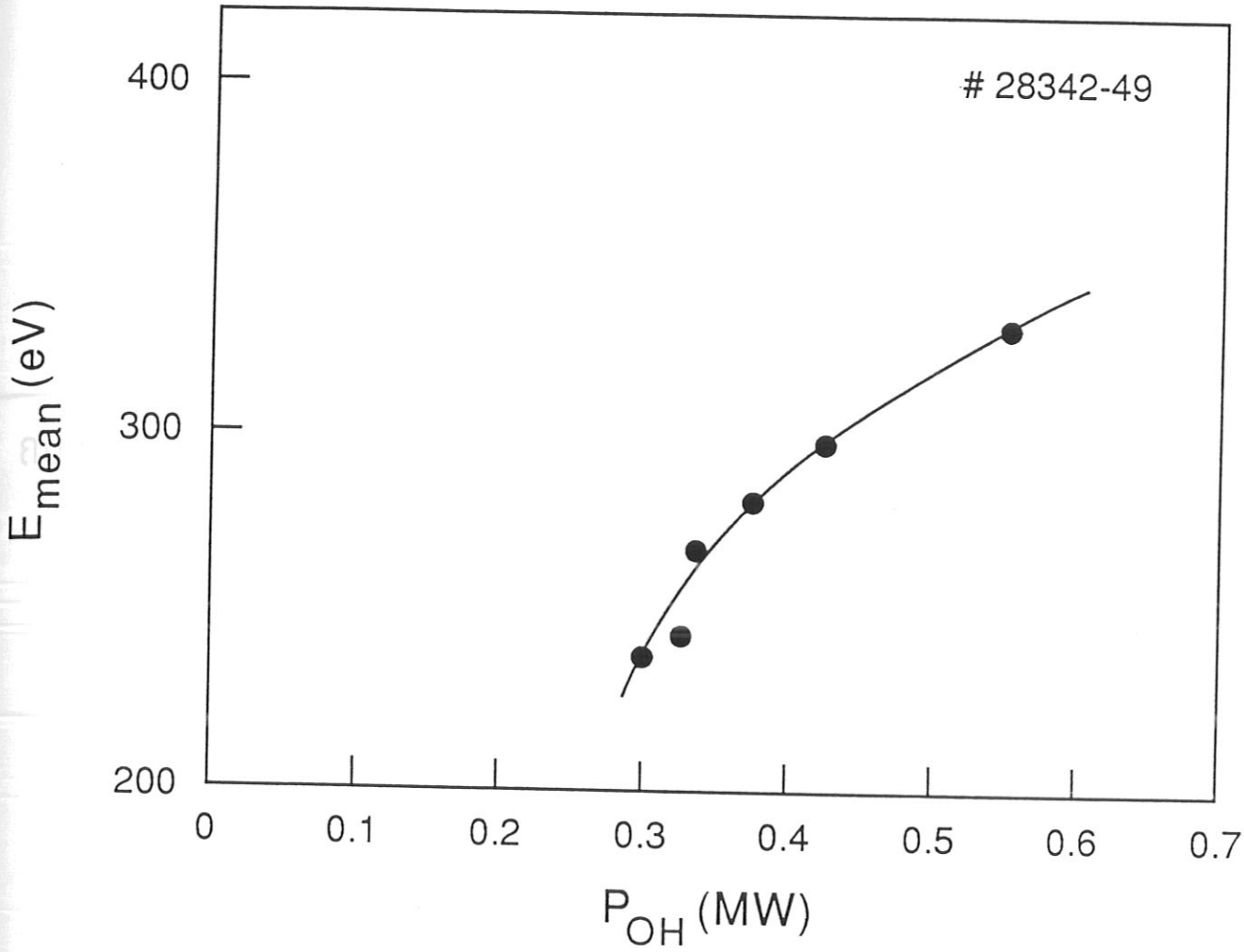

Fig.11: Mean energy of the CX-neutrals vs. Ohmic heating power.

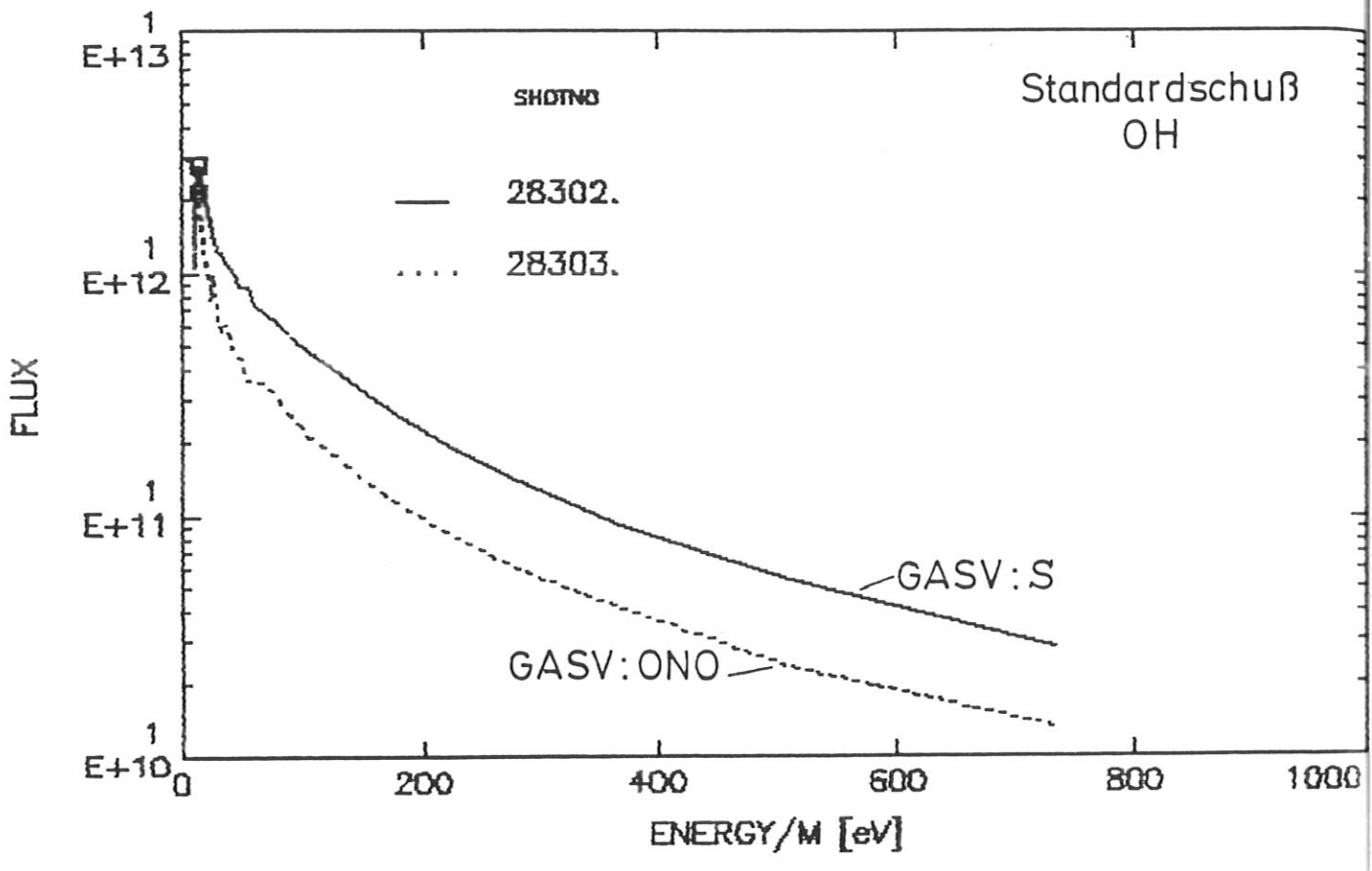

Fig.12: dΓ/dE for location of the external gas valve in the S and ONO sectors of ASDEX.

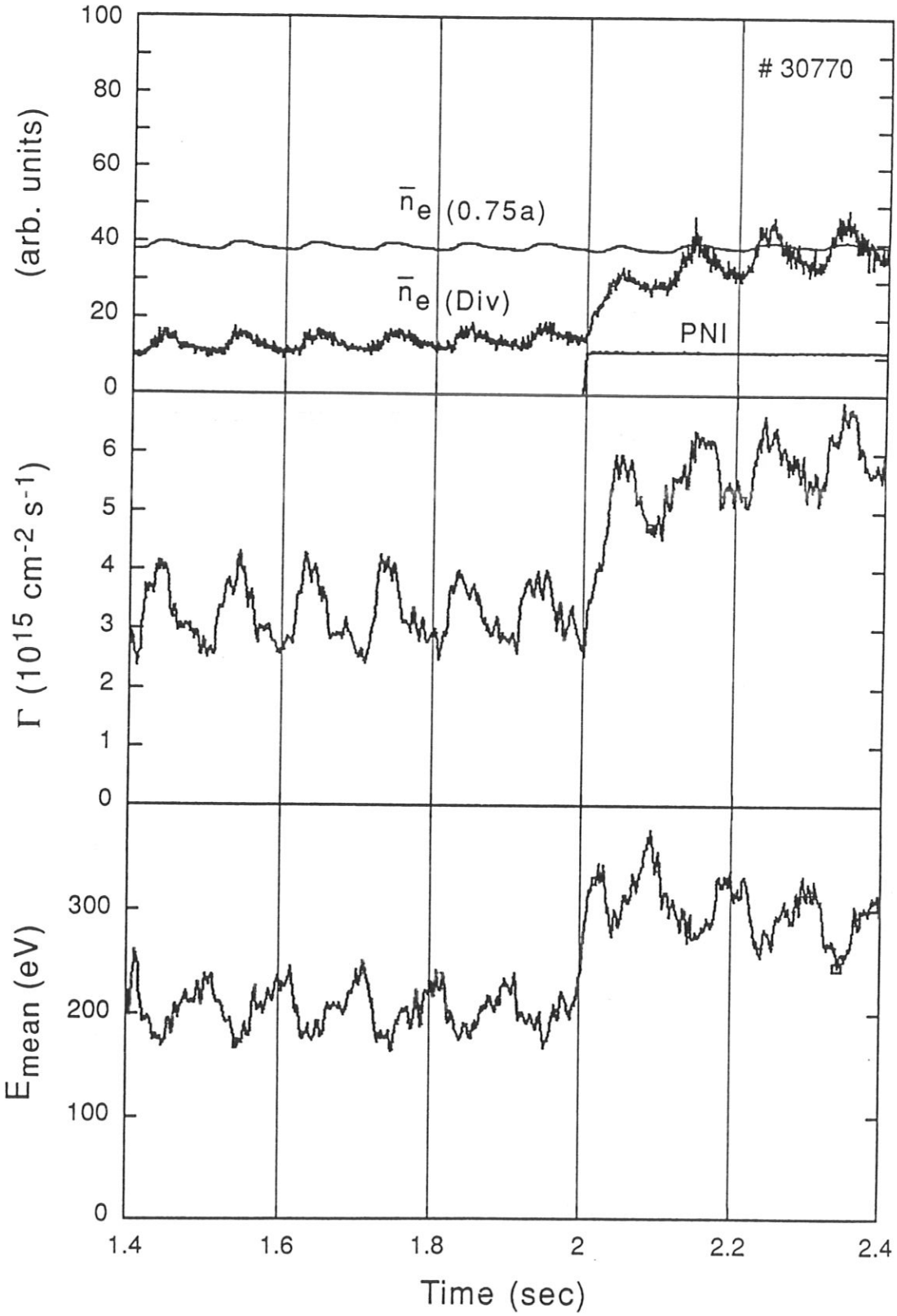

Fig.13: Gas oscillations. Upper Fig.: line averaged densities in the edge of the main chamber $\bar{n}_e$(0.75 a) and in the divertor chamber $\bar{n}_{eD}$; Centre Fig.: CX-flux Γ; Lower Fig.: E_{mean} of CX-neutrals. At 2 s is the onset of the neutral injection heating.

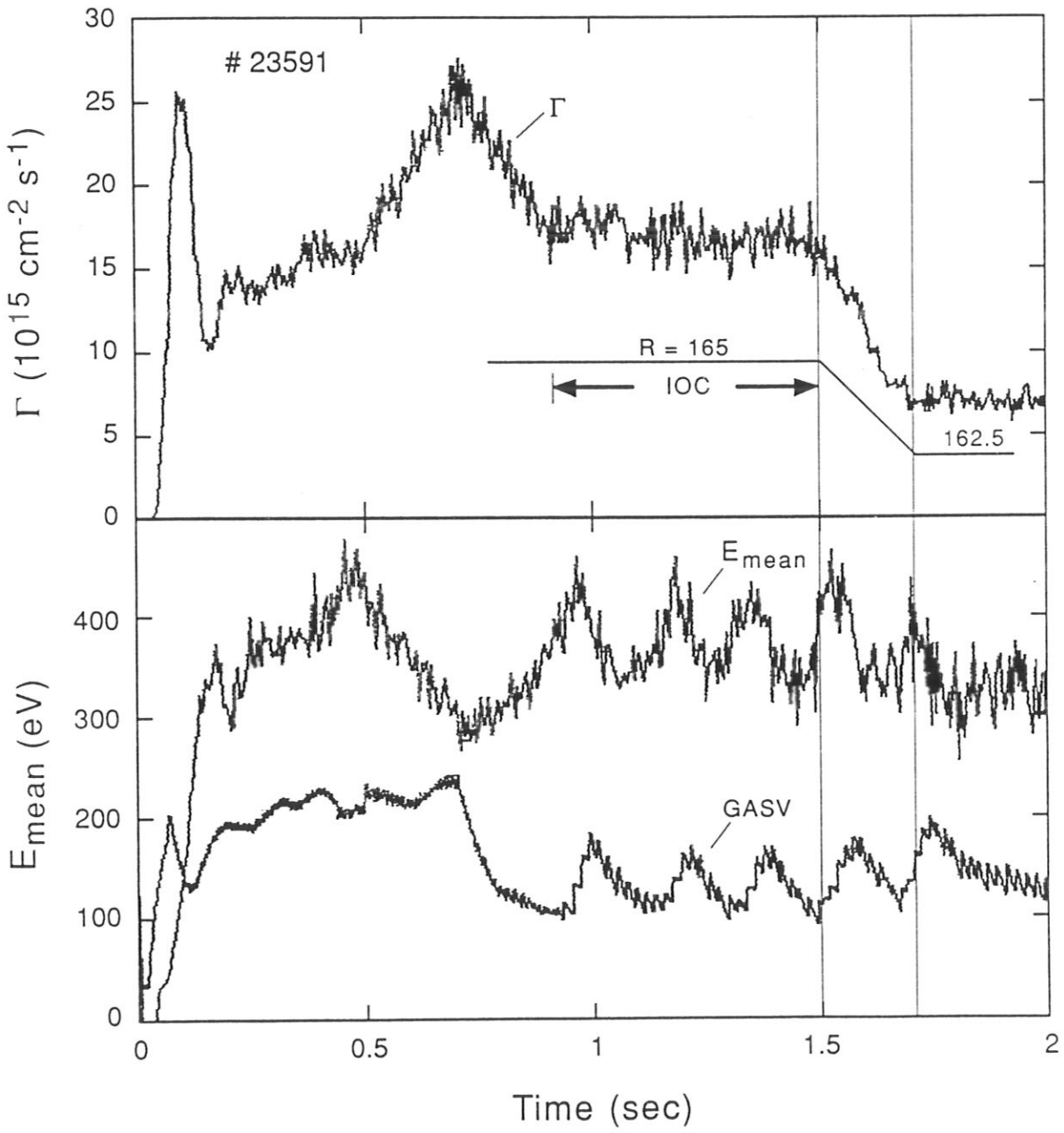

Fig.14: Gas oscillations during and IOC-shot.
The CX-Flux Γ (uppermost trace), its mean energy $\overline{E}$, and the voltage at the controlled gas valve (GASV). (At 1.5 s the plasma was shifted inward to R_{pl} = 162.5 cm).

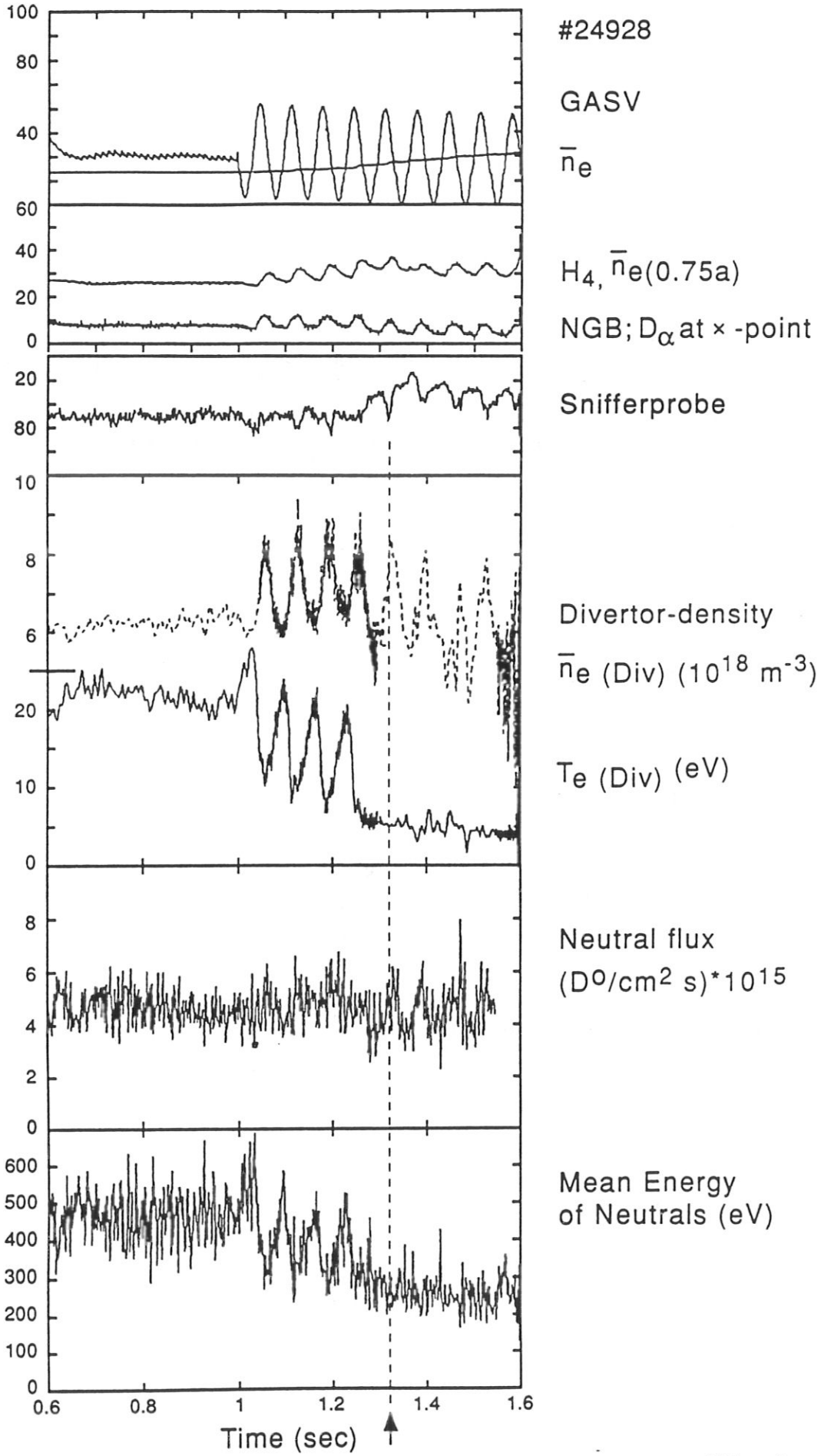

Fig.15: Various signals during a shot with gas oscillations (see text for details).

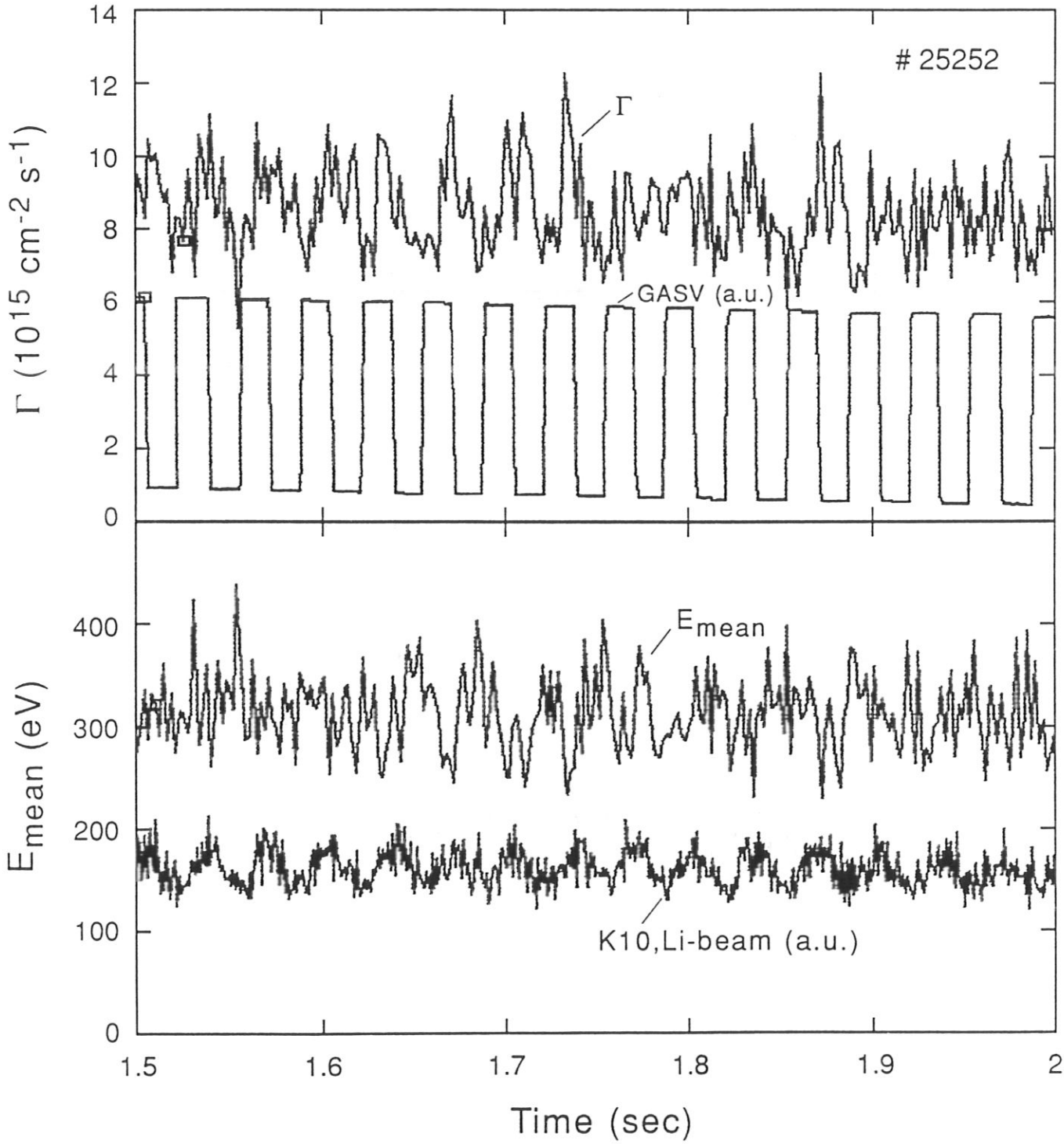

Fig.16: Gas oscillations. CX-Flux Γ, voltage at the gas valve (GASV), $\overline{E}$ of CX-neutrals, and signal K10 of the outermost channel of the Li-beam diagnostic.

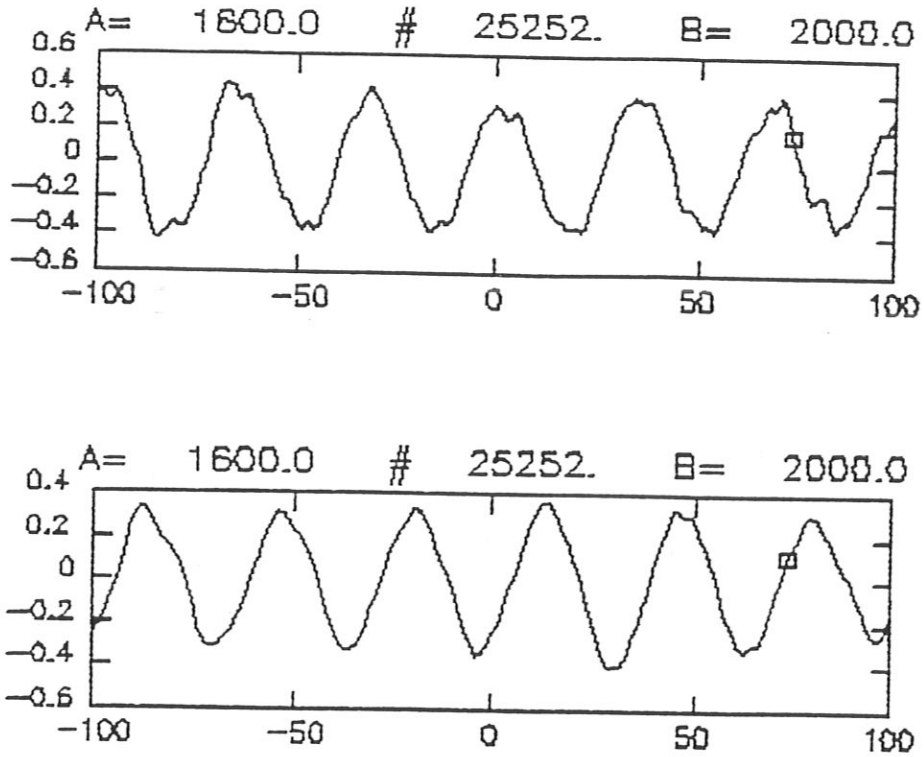

Fig.17: Cross correlation functions of a)Γ with K10 and b) $\overline{E}$ with $\overline{n_e}$ (0.75 a) for the shot of Fig.16.

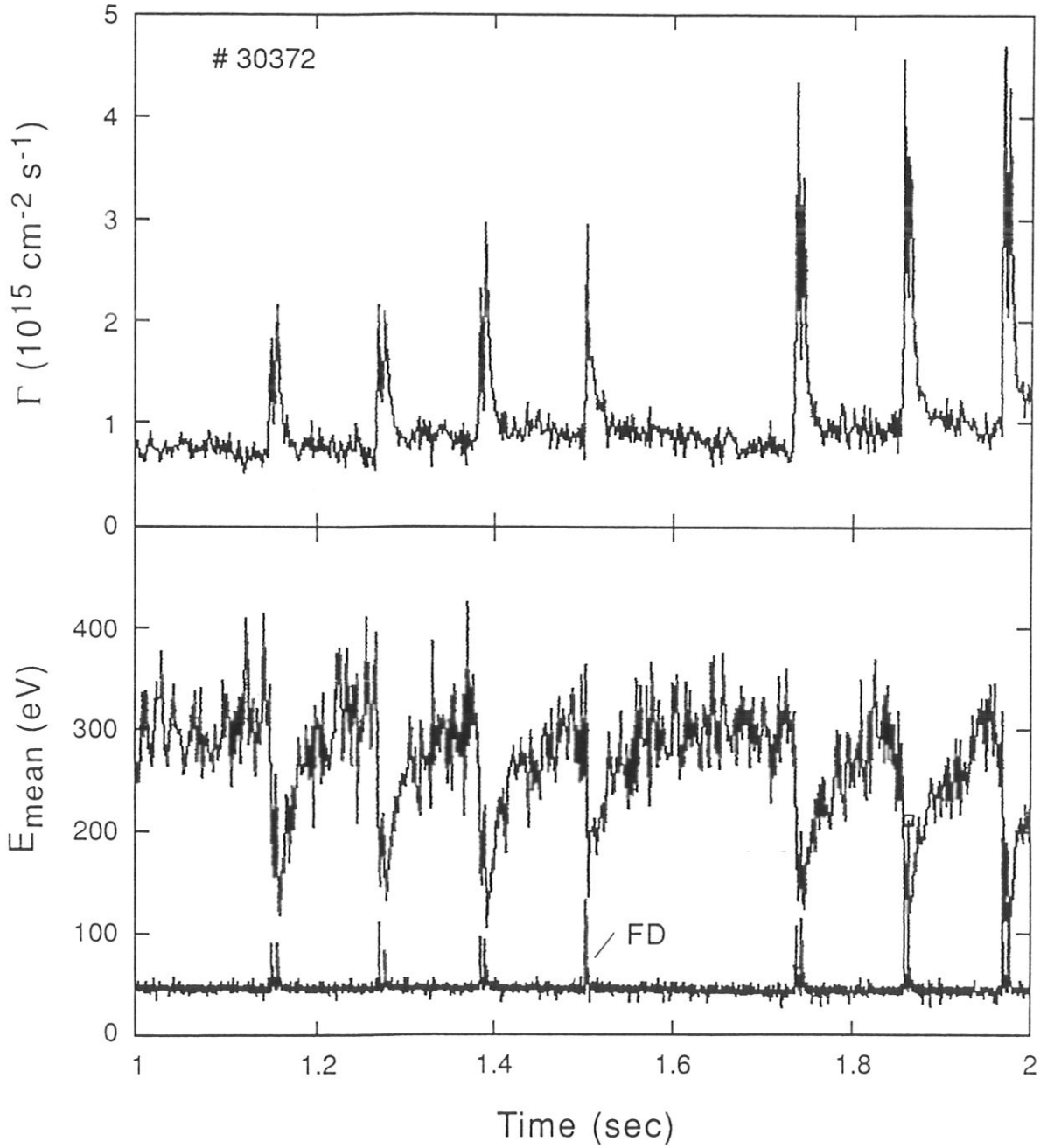

Fig.18: Response of the CX-flux Γ (upper trace), its mean energy E_{mean} (centre) on the injection of small D_2 pellets. The injection times are indicated by the spikes in the FD-signal (lowest trace).

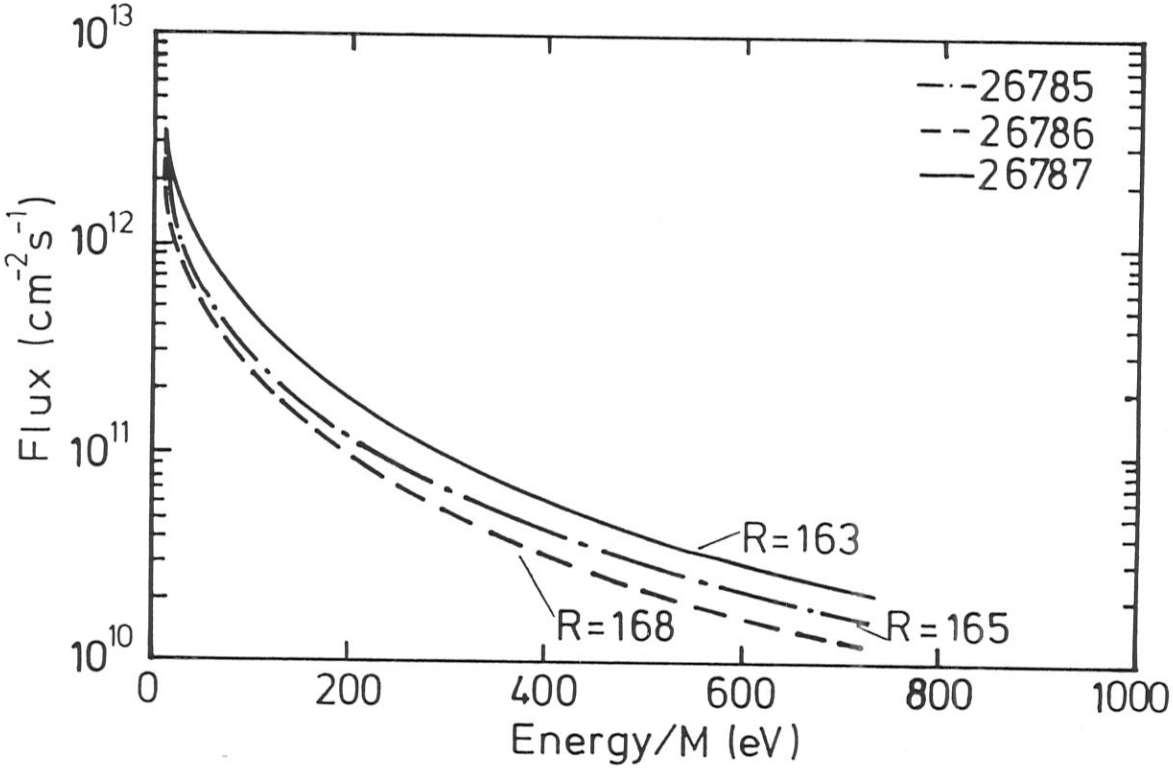

Fig.19: dΓ/dE for standard discharges with different plasma major radii R. (LENA-S).

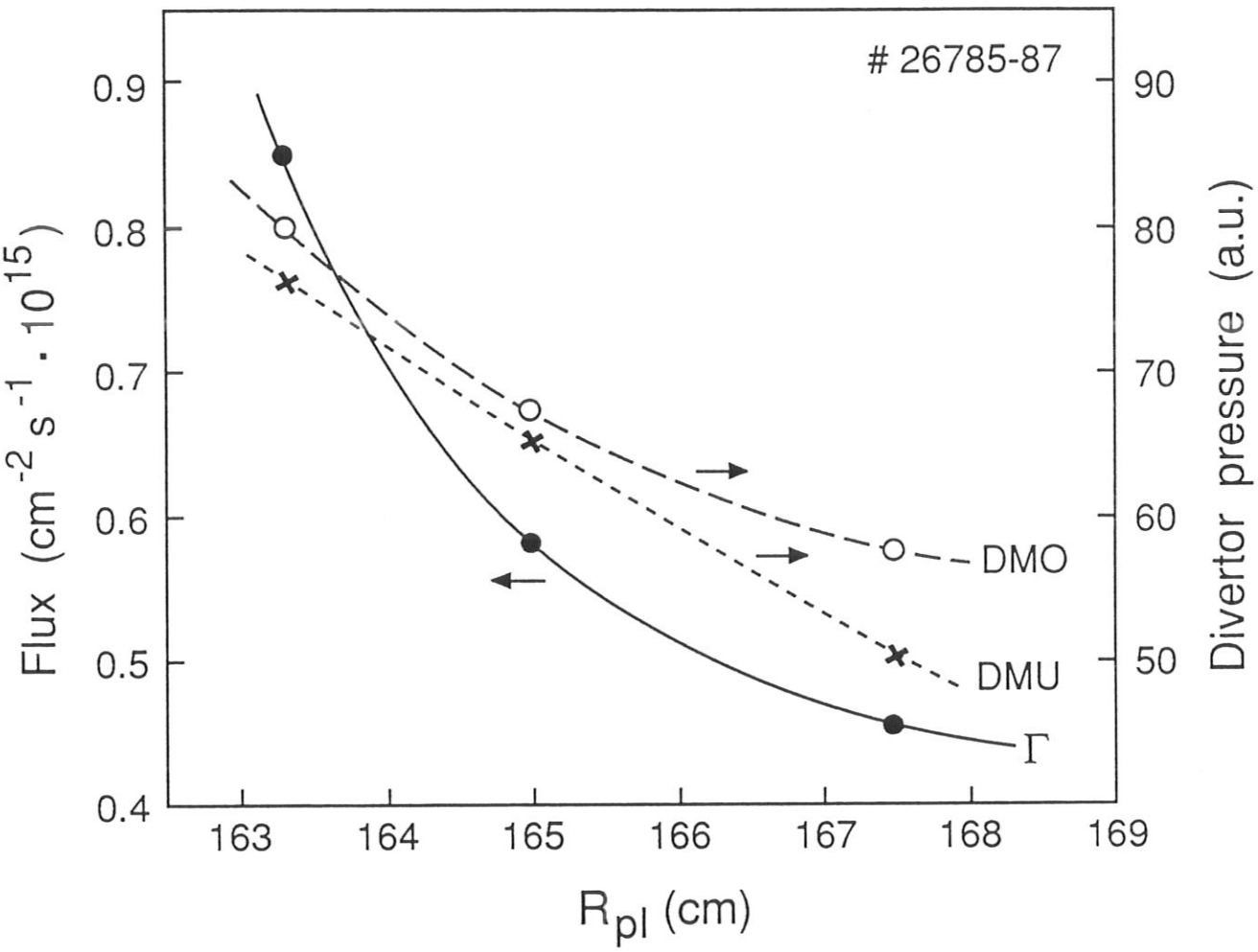

Fig.20: CX-Flux Γ, and pressures in upper (DMO) and lower (DMU) divertor chambers vs. major plasma radius R_{pl}.

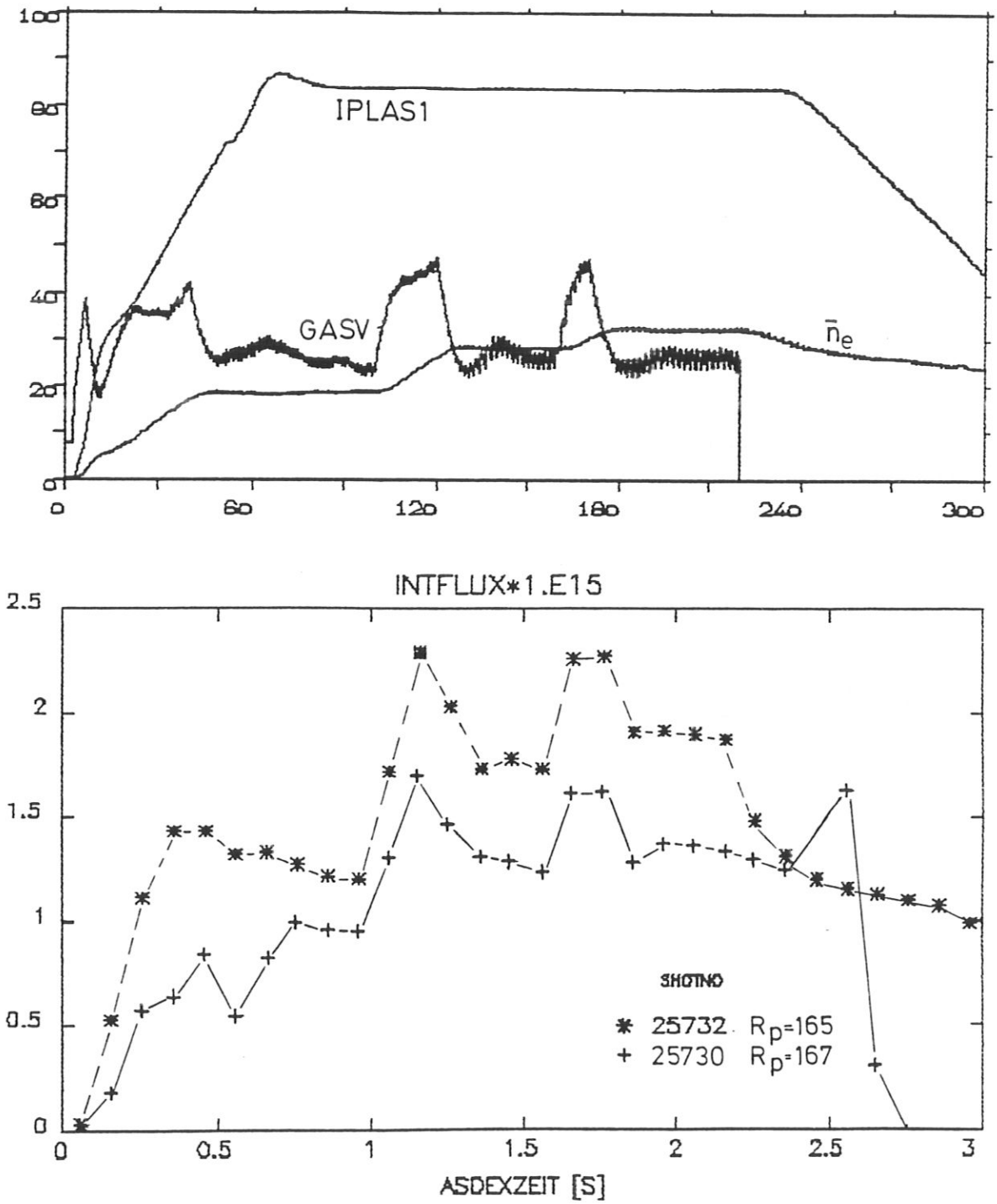

Fig.21: In both shots # 25730 and # 25732 were J_{pl} and $\bar{n}_e$ as in the upper figure. The lower Fig. shows Γ for 2 plasma radii R_{pl}.

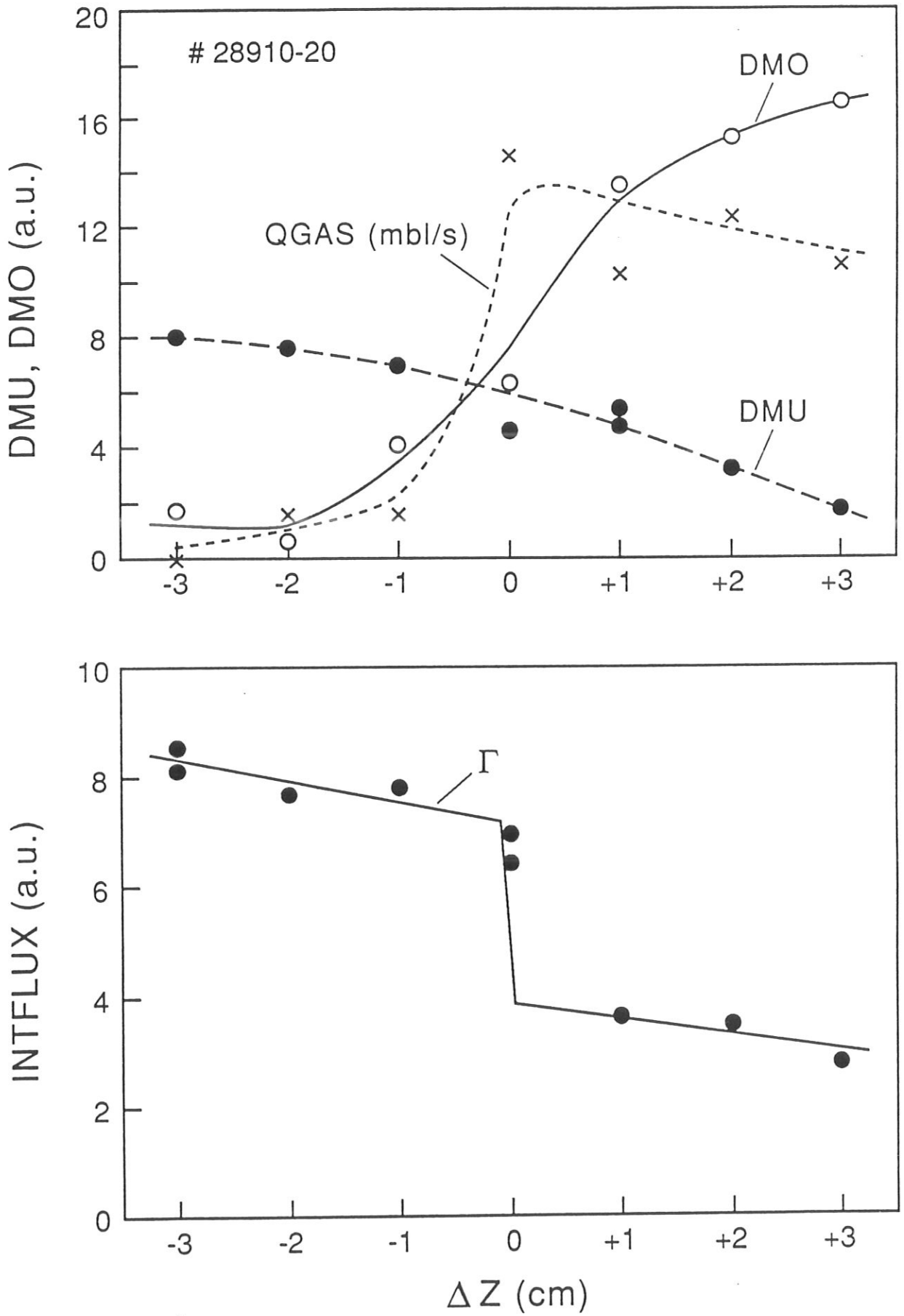

Fig.22: Γ as measured with LENA-S in its lowest position ($\alpha = 28^{o}$, see fig. 3) vs vertical plasma shift. In the upper part the pressure in the upper (DMO) and lower (DMU) divertor chambers and the gas puff rate are given.

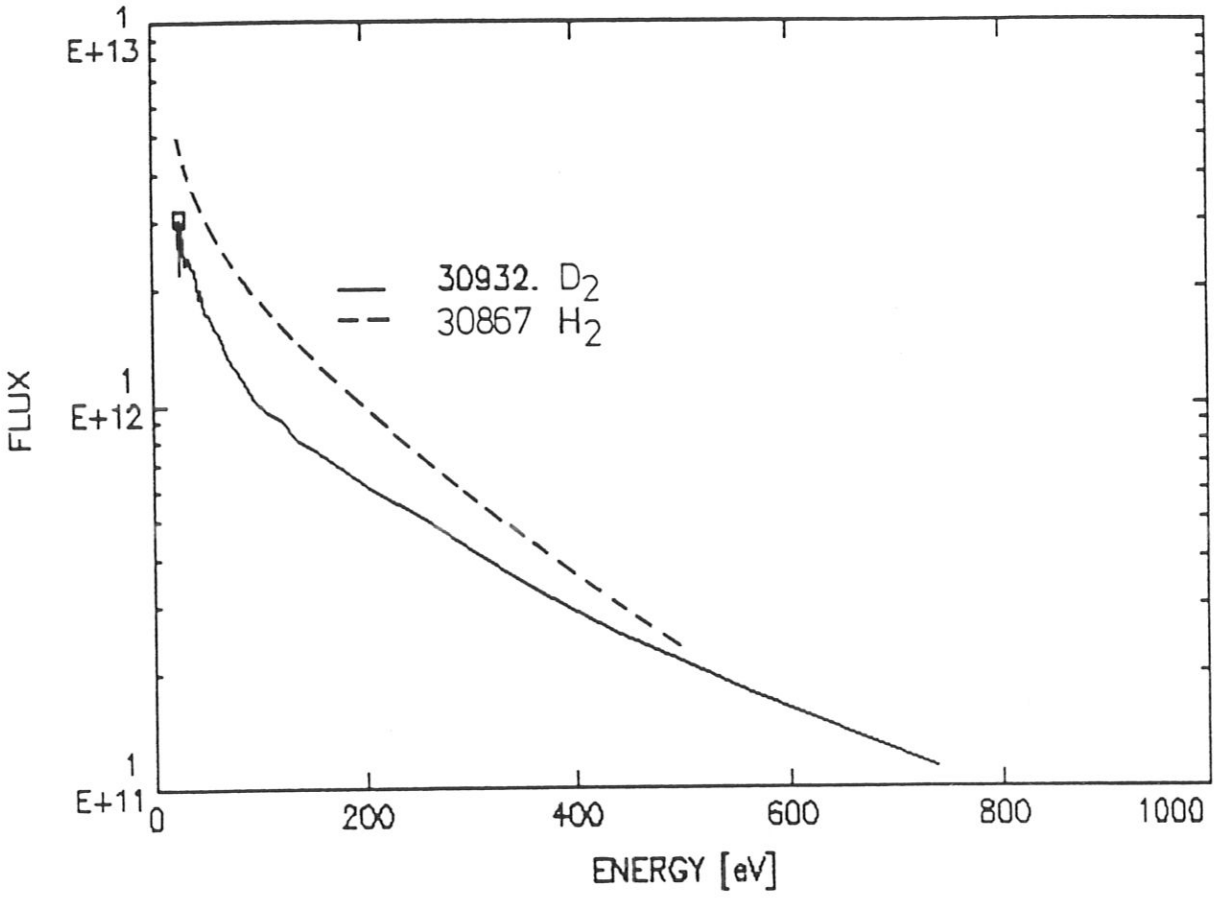

Fig. 23: Comparison of the CX energy distributions for standard H_2 and D_2 discharges.

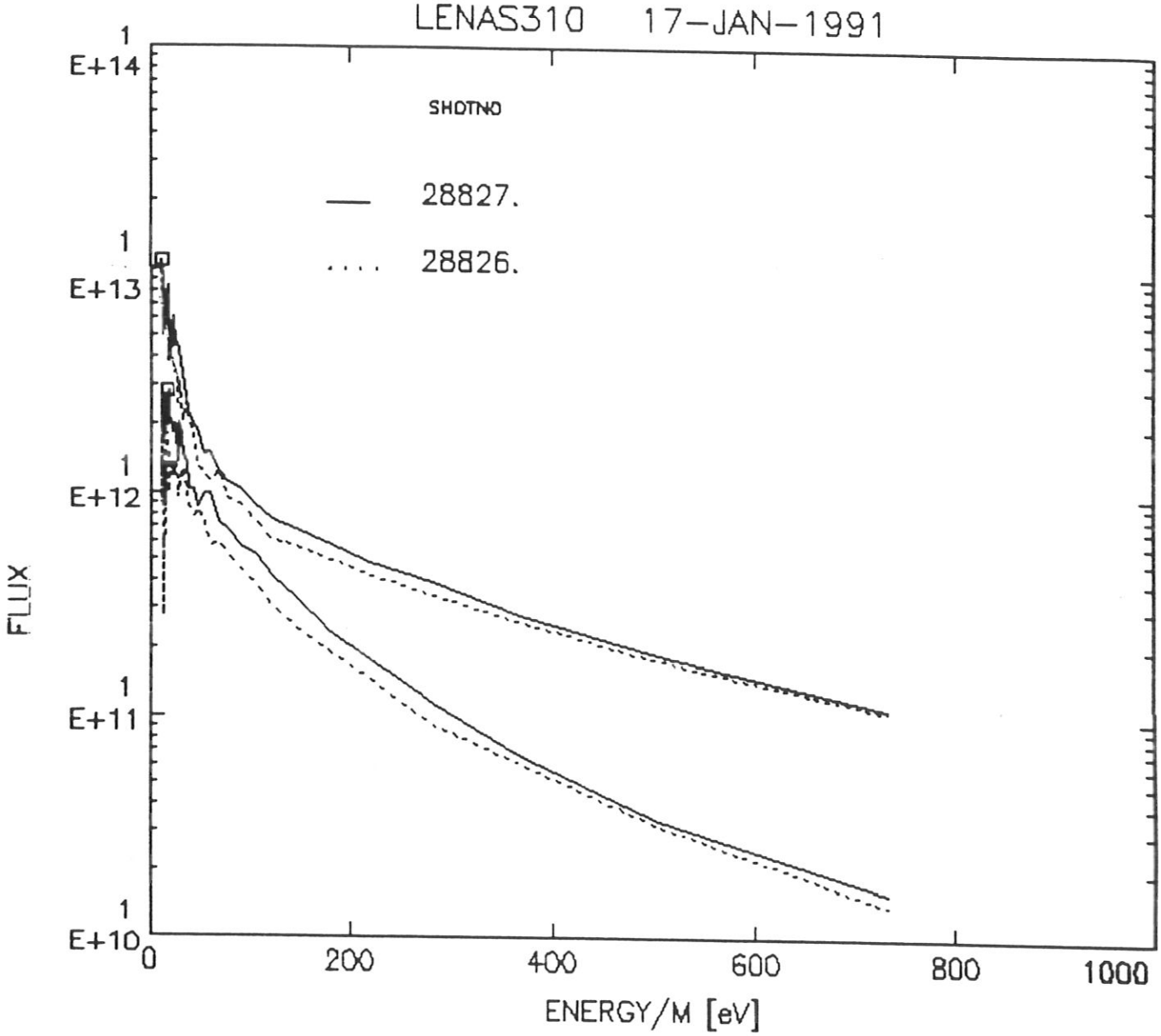

Fig.24: Comparison of dΓ/dE for # 28826 (sawtooth-free)with # 28827 (with sawteeth) for the Ohmic (upper fig.) and NI heated (lower fig.) phases.